Organic Geochemistry (in press)

Biogeochemistry of intertidal microbial mats of Qatar: new insights from organic matter characterization

Mirosław Słowakiewicz[a,b,c], Fiona Whitaker[d], Lisa Thomas[e], Maurice E. Tucker[d], Yanhong Zheng[a,b,f], Przemysław Gedl[g], Richard D. Pancost[a,b]

[a]Organic Geochemistry Unit, School of Chemistry, University of Bristol, Cantock's Close, BS8 1TS, UK

[b]Cabot Institute, University of Bristol, Cantock's Close, Bristol, BS8 1UJ, UK

[c]Polish Geological Institute, ul. Rakowiecka 4, 00-975 Warszawa, Poland

[d]School of Earth Sciences, University of Bristol, BS8 1RJ, UK

[e]Department of Biology, Bath Spa University, Newton Park, Newton St Loe, BA2 9BN, UK

[f]State Key Laboratory of Continental Dynamics, Department of Geology, Northwest University, 710069 Xi'an, China

[g]Institute of Geological Sciences, Polish Academy of Sciences, ul. Senacka 1, 31-002 Kraków, Poland

Highlights

Bacterial-archaeal microbial mats with allochthonous algal and higher-plant material

Occurrence of lipid biomarkers controlled by autochthonous and allochthonous biomass

Diagenesis involved sulphate reduction, methanogenesis and carbonate precipitation

Early cementation or burial by lime mud crucial for organic matter preservation

Abstract

Understanding early organic matter alteration and preservation in marine carbonate-evaporite systems could improve understanding of carbon cycling and hydrocarbon source rock prediction in such environments. It is possible that organic-rich microbial mats are important contributors to preserved hydrocarbons, and to explore this we examined changes in lipid composition in such a mat from a mesohaline intertidal lagoon, eastern Qatar. The mat reaches > 5 cm thickness over a carbonate mud substrate, rich in seagrass, gastropods and other small bioclasts. Clear lamination, with distinct downward colour changes from green to pink to brown, reflects different microbial mat communities. The layers contain spheroids of probable dolomite, the precipitation of which was plausibly bacterially-mediated. Lipids [*n*-alkanes, fatty acids (FAs), hopanoids, isoprenoid hydrocarbons, dialkyl glycerol diethers (DAGEs), and isoprenoid (0 to 4) and branched (Ia to IIIa) GDGTs] reflect the diverse mat-building phototrophic, heterotrophic and chemoorganotrophic microorganisms, as well as some likely allochthonous material (i.e. steroids, *n*-alkanols, high molecular weight *n*-alkanes). The lipids clearly document the change in microbial community, with phytene being the predominant hydrocarbon in the phototrophic surface layer. Oxygen and pH drop significantly 0.2 cm below the mat surface, coincident with the predominance of Deltaproteobacteria and increased concentrations of archaeal and bacterial glycerol dialkyl glycerol tetraether lipids andC_{15}/C_{16} and C_{16}/C_{17} dialkyl glycerol ether lipids in the deeper layers. Archaeol, likely of methanogen origin, is most abundant in the deepest layer. Allochthonous inputs occur throughout the mat, including abundant steroids, especially dinosterol and dinostanol, that are possibly related to periodic algal (dinoflagellate) blooms in the Arabian Gulf. Both *n*-alkanes and *n*-alkanols appear to be derived from seagrass. Organic matter contents decrease in the deepest mat; this suggests an overall low preservation potential of OM in intertidal mesohaline-hypersaline mats of the Arabian Gulf, which in turn suggests that these are not the major source of hydrocarbons in microbially-dominated carbonate-evaporite systems.

Keywords: microbial mats, lipid biomarkers, selective preservation, early diagenesis, Qatar

1. Introduction

Evaporitic environments are one of the most important sedimentary settings for organic matter (OM) preservation, as evidenced by prolific hydrocarbon production from many evaporite-carbonate formations (Warren, 2006 and references therein). This arises not only from the unique reservoir properties of the depositional facies, but also from the production and early diagenetic transformation of OM and mineral diagenesis (e.g. Gautier et al., 1985; Wakeham and Ertel, 1988).

Emery (1956) and Evans (1966) showed that the organic carbon (OC) content of modern evaporitic deposits in the Arabian Gulf ranges from 0.5 to 1.5 %. Vita-Finzi and Phethean (1980) reported higher values, up to 3.34 %, for muds in the inlets of the Musandam Peninsula near the entrance of the Arabian Gulf. Shearman and Skipwith (1965) suggested that the mucilaginous jackets which surround most shallow-water carbonate grains could be the source of much of the kerogen in carbonate rocks. Although Nitti et al. (2012) explored the vertical changes in the microbial community in lacustrine stromatolites, only a few studies have explored the vertical variation in bacterial and archaeal communities in zones of carbonate and evaporite precipitation (Kenig et al., 1990; Kendall et al., 2002). Kenig et al. (1990), together with Baltzer et al. (1994), analysed the OM in shallow-water lagoonal and intertidal sediments in Abu Dhabi. Three different organo-sedimentary facies were distinguished, with distinct organic signatures that persisted after burial and which are related to the rate of change of sea level, substrate morphology and rates of sedimentation. Both Kenig et al. (1990), and later Kendall et al. (2002), pointed out the source potential of these microbial mats.

This study is a development of earlier data (Słowakiewicz et al., 2014) on the OM in intertidal microbial mats from Mesaieed, eastern Qatar (Fig. 1), formed at the distal edge of a mixed carbonate-evaporite system, with a view to giving a better understanding of the biogeochemical interactions and OM composition in such environments. The first reports on Qatar microbial mats were given by Illing et al. (1965) and Shinn (1972); however, these early investigations focused only on organic mat descriptions. Recently, Al-Thani et al. (2014) presented a more detailed microbiological description of a hypersaline microbial mat from Um Alhool sabkha (just 1 km north of the site discussed here) and concluded that halobacteria and eukaryotes were predominant in all mat layers. However, there is uncertainty regarding early diagenetic changes in the OM composition of these mats and thus the preservation potential of hydrocarbons.

We describe here the environmental setting of the Mesaieed microbial mats, integrating detailed observations of their elemental, mineralogical, and optical microbiological composition, as well as the shallow surface water and pore water hydrochemistry, to evaluate how these control OC preservation. We evaluate the degree to which specific microbial communities in the different layers of a microbial mat give rise to differences in lipid biomarker distribution. Such profiling allows us to explore the primary generation of OM by cyanobacteria and other phototrophs and the fate of these compounds on burial within an environment rich in aerobic heterotrophs and sulphate-reducing bacteria (SRB), as well as utilisation of microbial products such as sulphide by phototrophic purple sulphur bacteria and autotrophic colourless sulphur bacteria. We also comment on the diagenetic degradation and transformation of OM in the intertidal mesohaline mat system.

2. Geological and hydrological setting

The Qatar Peninsula lies at 25°N and extends northward into the Arabian Gulf from the northeastern coast of the Arabian Peninsula (Fig. 1). The area experiences mild winters and very hot humid summers. Although the mean annual temperature is only 25 ºC, in the summer the mean daily temperature is commonly 30-35 °C, and during this period surface temperature can exceed 50 °C. Although summers can be humid, the area is very arid, with a mean rainfall of only 77 mm yr^{-1}, much of which occurs as rare high intensity events (Lloyd et al., 1987).

The Mesaieed sabkha is in the southeast of Qatar, to the south of Al-Wakra. It is the northern part of Qatar's largest coastal sabkha which extends southwards for ca. 60 km towards the border with Saudi Arabia. It sits at the northernmost limit of the country's remaining mobile barchan dunes, at the transition between oblique and leeward coastlines with respect to the dominant Shamal wind (Strohmenger and Jameson, 2015). The wind sources the siliciclastic sediments which comprise the major part of the sabkha, although detrital carbonate, shell material and pedogenic grain coatings also occur. The sabkha consists of an onlap wedge of Holocene sediments up to 15 m thick, which have prograded up to 6 km over Eocene carbonate strata of the Dammam Formation over the last ca. 6000 yr (Strohmenger and Jameson, 2015). The Holocene sediments are in hydraulic continuity with both offshore seawater and meteoric groundwater within the updip Eocene aquifer. Solar insolation drives evaporation from the shallow water-table and generates sabkha pore-fluids with salinity up to 300 ‰, from which pore-occluding and displacive gypsum is precipitated (Whitaker et al., 2014).

At Mesaieed, the periodic generation of chenier beaches during the late stages of the Holocene transgression resulted in the development of a series of spits extending south from the northern edge of a topographic low in the Eocene bedrock (Strohmenger and Jameson, 2015). The seaward part of this spit system defines the modern coastal margin of the Mesaieed sabkha. In a number of places, breaches of this low barrier have occurred, and the sea has inundated the back-barrier area, forming protected low-energy lagoons and ponds. In the Mesaieed area these are typically quite narrow (100-500 m), are elongated parallel to the coastline and connect with the sea via narrow inlets with tidally-reversing currents. Tidal variation in seawater head (1-2 m, Strohmenger and Jameson, 2015) gives rise to semidiurnal flooding and draining of the lagoons with local seawater. Small ponds with a diameter of 5 to 30 m are located more distant from the tidal inlets and will be flooded less frequently.

In this part of the southern Arabian Gulf, restriction of seawater circulation and high evaporation rate give rise to seasonal variation in seawater salinity, which in near-shore environments proximal to the study site ranges from ca. 43 ‰ to 58 ‰. Within the lagoon the salinity varies spatially, with complex temporal patterns at a range of scales. Hydrological data from the sabkha indicate that the dominant direction of groundwater flow is from the sea towards the middle part, driven by evaporative lowering of the hydraulic head (Whitaker et al., 2014), so the lagoonal systems appear not to receive significant input of evaporated fluid from the adjacent sabkha to landward.

The lagoons are fringed by low-growing halophytic vegetation, climaxing in the development of narrow bands of mangrove (*Avicennia* sp.) near the top of the intertidal zone. Away from these vegetated areas, the low-relief surface is mantled by dark-coloured laminated cyanobacterial mats, which are best developed in the middle to upper intertidal zone within ponded areas between shallow tidal channels. The mats, typically 4-6 cm thick, are broken up into saucer-shaped polygons, the edges of which are upturned, tufted and darker in colour. The mats are developed upon carbonate muds containing bioclasts (Fig. 2)

and are in contact with the Mesaieed siliciclastic-carbonate sabkha at a depth of 4-6 cm. This coastal depositional environment is repeated along parts of the Arabian Gulf coast (e.g. Shinn, 2011), and comparable cyanobacterial mats have been described elsewhere from similarly restricted, low-energy areas of the intertidal zone (e.g. Alsharhan and Kendall, 2003).

3. Methods

3.1. Sample collection, description and preparation

Two representative mat samples were collected from within the intertidal zone of a restricted back-barrier coastal lagoon at a location some 2 km northeast of Mesaieed (Fig. 1). At the time of sampling the pond was isolated from the lagoon and the mat was submerged to a depth of 5 cm. The upper 1 cm exhibited clear and sharp colour differences and included a 1-2 mm tufted green upper layer, underlain by a thin (1-2 mm) pink layer, a thicker (5 mm) brown layer and beneath this a second thin (1-2 mm) pink layer (Fig. 2). The underlying unit was brown to black and was differentiated into three rather thicker (1 cm) layers. The shallowest (1-2 cm depth) was thick and pale brown; it was underlain by a layer which was black with brown streaks (2-3 cm depth), and the basal layer unit was black (3-4 cm depth). The upper 5 cm of the underlying intertidal sediment is a pale coloured carbonate mud containing plant debris and *Cerithium* and *Monacha* (gastropods) shells. The plant material belongs to the seagrass species *Halodule uninervis* and includes rootlets. This is a common species in the gulf, characterised by a high tolerance to extreme conditions of salinity (38-70 ‰) and a temperature range of 10–39 °C. Pollen grains and leaf remains from this plant, in various states of preservation, were abundant in the carbonate bed, as well as being scattered within the layers of the microbial mat itself. The carbonate mud layer was rich in peloids and contained more cerithid gastropods, as well as Ostracoda and benthic foraminifera, including peneroplids, which are a typical seagrass meadow foram. Peloids several 10 μm in diameter occur scattered within the mat. The substrate for the microbial mat may well have been a seagrass meadow originally.

3.2. Hydrochemical analysis

In situ measurements of specific electrical conductance (SEC, ± 0.1 mS cm^{-1}), pH (± 0.01), temperature (± 0.1 ^{o}C), and dissolved O_2 (± 0.1 %) for the lagoon water overlying the mat were taken using a Hach multi-parameter instrument at the time of the sampling in June 2013, and also on a subsequent visit in January 2014. The latter provided an opportunity for subsurface characterization of pore waters, with *in situ* measurements at 1 cm depth intervals through the mat, and into the underlying sediment to a maximum depth of 15 cm. Salinity (PSU) was approximated from SEC using the relationship of Fofonoff (1985) extended to high salinity. Depth integrated samples were collected from the shallow lagoon at the sampling site, and mat pore water and sediment pore water were extracted under pressure in the field using a series of 10 cm diameter cores in 1 cm depth increments through the mat to a depth of 6 cm, and 3 cm increments below this. Local seawater was also sampled on a number of occasions through the year, as part of a wider study of the updip sabkha (Whitaker et al., 2014).

Alkalinity (as HCO_3^-) was determined using inflection-point (Gran) titration with 0.01 M HCl (precision ±0.5 %). Samples for cation and anion analysis were filtered through 0.22 μm membrane filters and stored at <4 ºC in high-density polyethylene (HDPE) bottles. All the samples were weight diluted before being analysed for major cations (Na^+, Ca^{2+}, Mg^{2+}, K^+) and anions (Cl^- and SO_4^{2-}) using inductively coupled plasma optical emission spectrometry

(ICP-OES) and UV-VIS spectrophotometry respectively. Analyses give a combined ion balance error of 1.9 % ± 3.9 %. $_pCO_2$ and saturation indices (log IAP/K) for carbonate and evaporite minerals were calculated with PHREEQC version 3 using the Pitzer equation for calculation of solute activity (Parkhurst and Appelo, 2013).

A minimum of 2.7 ml of raw pore fluid sample from the mat was treated with 10 % glutaraldehyde on the day of sampling to facilitate preservation of bacteria. The treated sample was allowed to rest for 15 min in the absence of sunlight after staining with 5 % gold.

3.3. Microbiological analysis and mat description

A sample of the mat was frozen immediately after collection and maintained frozen in transit to the University of Bristol. It was subsequently defrosted, dissected, again frozen and freeze-dried prior to analysis. Using a dissecting microscope (Nikon SMZ645), a 5-cm thick sample of the defrosted live mat was split into 7 transverse sub-sections, retaining the original surface orientation and being of contrasting character (Fig. 2). Each was placed in a sterilised Petri dish containing artificial seawater (ASW) made from a recipe supplied by the Culture Collection of Algae and Protozoa (CCAP). The sub-sections were stored in an environmental chamber at 21 ºC, day neutral i.e. 12 h light, 12 h dark. The mat sections were examined and species identified using a light microscope (Nikon Labophot 2A). A number of biological and geological staining techniques were applied in order to identify mineral inclusions within the mat, using methods based on those described by Friedman (1959) and Lindholm and Finkelman (1972). The obtained results were integrated with DNA and pyrosequence data reported by Al-Thani et al. (2014) from microbial mats located 1 km to the north.

3.4. Mineralogy

Titan Yellow, which stains grains red if they contain Mg (Tucker, 1988), was used on selected mat samples. All powdered mat samples were analysed with X-ray diffraction (XRD) to determine the mineralogy. Following the identification of dolomite (see later section), the samples were prepared for scanning electron microscopy (SEM; JEOL SEM5600 LV) by first dissolving out the OM using a 10-15 % sodium hypochlorite (bleach). The residue was shaken and after a few s, when the coarser material had settled to the bottom of the beaker, a small piece of glass (2 cm square) on a wire frame was lowered into the beaker and the material still in suspension was allowed to settle on the glass. After 15 min, when the solution was clear, the glass was removed and allowed to dry. The particles on the glass were all < 5 μm, the typical maximum size of carbonate precipitated in microbial mats (e.g. Bontognali et al., 2010).

3.5. Elemental and isotopic analyses

Elemental analysis was carried out on all dissected mat layers including the underlying carbonate unit. Total carbon (TC) content (± 0.2%) was obtained from the powdered samples using a EUROVECTOR EA3000 Elemental Analyser. Total inorganic carbon (TIC) was determined (± 0.1%) as carbonate using a CO_2 coulometer (a modified Strohlein Coulomat 702 Analyser). Total OC (TOC) values were calculated as the difference between TC and TIC. Total S (TS) content (± 0.1%) was obtained with a CARLO ERBA NC2500 Elemental Analyser, whereas total N (TN) analysis (± 0.1%) was carried out with a EUROVECTOR EA3000 Elemental Analyser. Total P (TP, ± 0.05%) was determined with a UV/Vis spectrophotometer.

Several preliminary carbon and oxygen isotope analyses were obtained for the carbonate

within the mat and the underlying lime sediment. The carbon and oxygen isotopic compositions of carbonate carbon were determined using the following procedure: 100-200 µg powdered carbonate were placed into 4 ml glass vials and then sealed by a lid and pierceable septum. The vials were placed in a heated sample rack (90 ^{o}C) where the vial head space was replaced by pure He via an automated needle system as part of an Isoprime Multiflow preparation system. Samples were then manually injected with ca. 200 µl H_3PO_3 and left to react for at least 1.5 h before the headspace gas was sampled with an automated needle and introduced into a continuous-flow Isoprime mass-spectrometer. Duplicate samples were extracted from each vial, and a mean value obtained for both $\delta^{13}C$ and $\delta^{18}O$. Samples were calibrated using the IAEA standards NBS-18 and NBS-19, and values are reported as ‰ on the Vienna Peedee belemnite (VPDB) scale. Reproducibility within runs was 0.09 ‰ for $\delta^{18}O$ and 0.05 ‰ for $\delta^{13}C$.

3.6. Lipid analysis

The freeze-dried samples (1-2 g) were ground using a glass mortar and pestle and extracted using a modified Bligh-Dyer monophase solvent system containing buffered water (0.05 M KH_2PO_4; pH 7):$CHCl_3$:MeOH (4:5:10, v/v/v). $CHCl_3$ and buffered water were added to the supernatant to separate the organic phases from the solution. All extracts were combined to yield the total lipid extract (TLE). An aliquot of the TLE was separated into simple lipid, glycolipid and phospholipid fractions using silica column chromatography with $CHCl_3$:HOAc (99:1, v/v), Me_2CO and MeOH, respectively (Dickson et al., 2009). The simple lipid fraction was separated into neutral and free fatty acid (FA) fractions using silica column chromatography with $CHCl_3$ saturated with NH_4OH and $CHCl_3$:HOAc (99:1, v/v), respectively. 5α-Androstane and hexadecan-2-ol (200 ng) were added to the neutral fraction as internal standards. This fraction was separated into neutral apolar (containing hydrocarbons) and neutral polar (containing *n*-alkanols, hopanols, sterols, stanols, bacterial dialkyl glycerol diethers (DAGEs), archaeol, glycerol dialkyl glycerol tetraethers (GDGTs)) fractions by elution through an activated Al_2O_3 column with hexane/dichloromethane (DCM) (9:1 v/v) and DCM/MeOH (1:2 v/v, respectively).

The FAs were methylated using BF_3/MeOH (100 µl) at 70 ^{o}C for 1 h. The methyl esters were extracted with DCM (3 x 2 ml) and the combined extracts dried under N_2. The FA methyl esters (FAMEs) were dissolved in DCM (ca 1 ml) and eluted through a pre-washed anhydrous Na_2SO_4 column to remove residual water.

Phospholipid and glycolipid head groups were cleaved by way of acid hydrolysis of ester bonds using 5 % HCl in MeOH, and the products were mainly phospholipid FAMEs (PLFAMEs) and glycolipid FAMEs (GLFAMEs). An *n*-C_{19} standard was added to the FA, phospholipid and glycolipid fractions and the solvent removed under N_2.

All fractions (except the neutral apolar fraction) were derivatised with pyridine (20 µl) and bis(trimethylsilyl)trifluoroacetamide (BSTFA; 20 µl, 70 ^{o}C, 1 h) to form trimethylsilyl derivatives of hydroxyl moieties.

Neutral apolar fractions were analysed using gas chromatography-mass spectrometry (GC-MS) with a ThermoQuestFinnigan Trace GC and MS instrument equipped with a non-polar silica CP Sil5-CB column (50 m x 0.32 mm i.d., 0.12 µm film thickness) using the following programme: 70 ^{o}C to 130 ^{o}C at 20 ^{o}C/min, then to 300 ^{o}C (held 10 min) at 4 ^{o}C/min. The ionisation potential was 70 eV, with the scan range *m/z* 50-650. Acid-hydrolysed glycolipid and phospholipid, free fatty acid and polar fractions were analysed with the same GC-MS instrument equipped with a Varian Factor Four VF23MS column (60 m x 0.32 mm,

0.15 µm) using the following programme: 70 ^{o}C to 130 ^{o}C at 20 ^{o}C/min, then to 250^{o}C (held 10 min) at 4^{o}C/min.

The polar, phospholipid and glycolipid fractions, containing GDGTs, were analysed using high performance liquid chromatography-atmospheric pressure chemical ionisation-MS (HPLC-APCI-MS; Thermo ACCELA LC-MS Thermo-Quantum Access MS instrument) and separation with an Alltech Prevail CyanoColumn (150 mm x 2.1 mm; 3 µm i.d.), following the method of Schouten et al. (2007). The injection volume was 15 µl and the elution gradient was 99 % hexane and 1 % isopropanol, isocratically for the first 5 min, followed by a linear gradient to 1.8 % isopropanol over 45 min, with a constant flow rate of 0.2 ml/min. Analyses were performed using selective ion monitoring (SIM; *m/z* 1302, 1300, 1298, 1296, 1294, 1292, 1050, 1048, 1046, 1036, 1034, 1032, 1022, 1020 and 1018) to increase sensitivity and reproducibility, and $[M+H]^+$ ions were integrated. The column was re-equilibrated following each analysis. The relative response ratio of the GDGTs to the internal C_{46} GDGT standard was set at 1:1, allowing semi-quantitation.

3.7. Palynology

Mat samples were divided into two parts: 0-3 and 3-5 cm; an aliquot (10 g) of each was treated with cold 36 % HCl to remove carbonate, and with cold 34 % HF to remove silicate. The residuum was sieved at 10 µm on a nylon mesh, and separated from undissolved particles using heavy liquid separation ($ZnCl_2$+HCl; 2.0 g/cm^3) and divided into two parts. One was treated for 10 s with fuming HNO_3, the second one was left untouched for analysis. Both residues were studied for palynology using the light microscope.

3. Results and discussion

4.1. Hydrochemistry

Samples of shallow surface waters above the mat sampled in June 2013 and January 2014 had salinities 64.1 ‰ and 40.2-41.1 ‰, respectively, the former being significantly elevated relative to samples of local near-shore seawater (40.6-48.8 ‰) reflecting the effect of evaporation in the restricted lagoon (Fig. 3a). *In situ* subsurface measurements in June 2013 showed a linear reduction in salinity with depth, from 61.3‰ at 1 cm to 45.8 ‰ at the base of the mat, which was 5-6 cm thick at the location of water sampling. Salinity in the top 10 cm of the underlying sediment was 40.7 ± 1.6 ‰ (n=8, data not shown). This excludes a single anomalous reading of 32.2 ‰, which may possibly reflect the effect of antecedent rainfall, although inland of the lagoon all shallow groundwater samples have salinity elevated by shallow evaporation and dissolution of soluble salts (Whitaker et al., 2014).

The shallow water overlying the mat was highly alkaline, with pH 9.45 and 8.77-9.14 in June and January, respectively, compared to 8.16-8.23 for the local seawater. It was also characterised by very high daytime dissolved O_2 (290 % and 159-205 % saturation; Fig. 3a). This suggests that cyanobacterial photosynthetic activity at the surface of the mat modifies the composition of overlying water, with strong drawdown of CO_2 ($_PCO_2$ $10^{-5.46}$ atm and $10^{-4.22}$-$10^{-4.82}$ atm compared to atmospheric equilibrium values of $10^{-3.32}$-$10^{-3.60}$ atm) in the nearshore seawater (Fig. 3b), and generation of a high level of O_2 supersaturation (Fig. 3a). Differences between the June and January measurements relate to the timing of sampling relative to maximum solar insolation, as well as the degree of restriction, as indicated by the salinity. Given the shallow water depth above the mat, water chemistry likely shows a significant diel variation (Des Marais, 2003) and time of day likely exerts a strong control on pH and dissolved O_2; unfortunately we were not able to determine these parameters due to access restrictions.

Despite extreme O_2 supersaturation in the overlying lagoon water, dissolved O_2 levels declined dramatically in the very shallowest part of the mat, to 3.6 % at 1 cm depth and reached the limit of detection (0.1 %) at the base of the mat (Fig. 3a), at which value it remained through the maximum measured depth in the underlying sediment (data not shown). Given the relatively large diameter of the probe, this suggests that the system was anoxic beneath the surficial photosynthetic layer. The associated reduction in pH through the mat was more gradual, but by 2 cm pH had dropped below that of seawater, and reached 7.62 at the base of the mat. This trend continued within the sediment below, though with a more gradual rate of reduction with depth, to a minimum of 7.51 at the base of the profile (data not shown). This likely reflects the high CO_2 production by microbial metabolic reactions. The $_PCO_2$ of pore waters increases rapidly with depth, reaching $10^{-2.86}$atm by the base of the mat, three orders of magnitude higher than the daytime $_PCO_2$ in the overlying lagoon water (Fig. 3b). Porewater in the sediment beneath the mat was also equilibrated with an elevated $_PCO_2$ of between $10^{-2.70}$ and $10^{-2.37}$ atm (data not shown).

This variation in $_PCO_2$ affects saturation index (SI) with respect to key carbonate minerals (Fig. 3b). Surface water (daytime) above the mat was strongly supersaturated with respect to aragonite, calcite and dolomite, in excess of values for local seawater. The HCO_3^- alkalinity exceeded that of seawater, confirming the role of photosynthesis rather than precipitation of carbonate minerals in controlling the drawdown of CO_2. The maximum HCO_3^- alkalinity was observed in the upper 1 cm of the mat, with a value of 3.99 mmol, some 2.6 times that of the overlying lagoon water and 1.5 times that in the remaining part of the mat. Alkalinity then increased in the sediment beneath the mat to 3.45 ± 0.14 mmol at 15 cm (data not shown). The maximum degree of supersaturation with respect to carbonate minerals occurred in the uppermost sample from the mat (0-1 cm), reflecting the particularly high alkalinity, despite the low dissolved O_2 content. Beneath this, carbonate mineral SI declined with depth and approached aragonite equilibrium in the sediment that underlies the mat, with the sample from the pit in the siliciclastic sands beneath the pond being marginally aragonite-undersaturated. The dolomite SI followed a similar trend, varying over two orders of magnitude, but all samples remained dolomite supersaturated. In contrast, all samples were undersaturated with respect to gypsum (the dominant local evaporite mineral; Whitaker et al., 2014), as well as all other evaporite minerals.

4.2. Microbiology and palynology

Previous sequencing (Al-Thani et al., 2014) revealed that in related mats and throughout the mat profile, bacterial communities are dominated by Proteobacteria. However, this work also revealed the presence of eukaryotic microorganisms in the mat, albeit at subordinate abundances. Among the Archaea, *Crenarchaeota* dominate throughout that profile, but *Halobacterium* are the most abundant with subordinate contributions from *Methanosarcinales* and unidentified *Euryarchaeota* (Al-Thani et al., 2014). Here, we have examined mat microbial structure using microscopic observations, providing complementary insights. The surface of the mat to a depth of 0.2 cm was dominated by the cyanobacterium *Lyngbya aestuarii*, which has long, unbranching filaments inside a rigid mucilaginous sheath (Fig. 2). This non-heterocystous N_2-fixing species is a common constituent of surface layers of modern microbial mats in many hypersaline environments (e.g. Javor and Castenholz, 1981; Martinez-Alonso et al., 2004). *Lyngbya* has a pale brownish colour from the presence of scytonemin, a pigment produced in the sheath, which provides protection against damage by UV radiation (Proteau et al., 1993; Rath et al., 2012). Laminated mats with a surface layer dominated by *Lyngbya* are common where the surface is periodically flooded then desiccated;

this represents a pioneer mode of microbial mat, often characterised by relatively low species diversity (Omoregie et al., 2004; Balskus et al., 2011).

Partially mixed with the *Lyngbya* was a dense green layer (0-0.2 mm) of *Microcoleus chthonoplastes*, another non-heterocystous filamentous cyanobacterium. Both species are photosynthetic and capable of N_2 fixation. *Microcoleus chthonoplastes* also exhibits a variant type of photosynthesis. It is capable of using H_2S as an electron donor, which it can oxidise to $S_2O_3^{2-}$ (de Wit et al., 1988; Stal, 2012). Cyanobacteria in these upper few mm are the most important primary producers and generate O_2 enriching the overlying water and which can diffuse into the upper few mm of the mat.

Microscopic examination revealed the phototropic purple sulphur bacterium *Thiocapsa* as the major constituent of the 1 mm thick pink layer lying immediately below the oxic layer, yet within the depth of light penetration. It is generally an anaerobic bacterium, using reduced S as an electron donor during photosynthesis. It has spherical cells, 1-3 μm in diameter, commonly forming tetrads; it typically forms mm-thick layers within microbial mats in hypersaline locations (Martinez-Alonso et al., 2004), as observed here.

Beneath the strongly-laminated, surface oxic layers, from 0.3 cm to 2 cm, was a thicker series of pink to pale brown layers with clearer laminae, within which *Beggiatoa alba* and subordinate Alphaproteobacteria (0.3-0.8 cm) were found. *Beggiatoa alba* is a sulphur-oxidising bacterium with colourless filaments and formed a white, translucent to opaque layer at 0.8-1.0 cm depth, and also appeared to colonise fragments of plant debris in the mat. *Beggiatoa* is typical of habitats with a high level of H_2S, which is used as an energy source, forming intracellular S droplets which are reduced to S^{2-} under short-term anaerobic conditions (Schmidt et al., 1987; Berg et al., 2014). This quite thick (10-150 μm diameter) filamentous bacterium was surrounded by mucilage or extracellular polysaccharide (EPS). A pale brown layer (2-3 cm) was dominated by Deltaproteobacteria with subordinate *Chloroflexi*, *Spirochaetes* (Al-Thani et al., 2014), and the unicellular cyanobacterium *Synechococcus*; *Synechococcus* has been reported to thrive in hypersaline solar ponds (Roux, 1996; Madkour and Gaballah, 2012) and high temperature (60-65^{o}C) springs (Becraft et al., 2011). The underlying dark layers (>3 cm depth) comprise empty bacterial sheaths and deposits of orange/brown scytonemin, but more specific interpretation was not possible using only visual approaches. It is likely that dominant organisms in these layers include Thaumarchaeota (inferred from biomarkers, see Section 4.5.8), as well as Deltaproteobacteria, *Chloroflexi*, and *Spirochaetes* (inferred from molecular analyses at a nearby mat; Al-Thani et al., 2014). Using the Turnbull's Blue staining method (Dickson, 1966) Fe^{2+} was found within the EPS surrounding the scytonemin.

Total bacterial counts in pore water samples from the mat averaged $1.7 \pm <0.1 \times 10^7$ counts ml^{-1}, and were marginally lower than those from water samples from the underlying sediment ($2.8 \pm 1.7 \times 10^7$ counts ml^{-1}).

Each layer of the mat yielded rich palynological material composed chiefly of seagrass remains and structureless material associated with aquatic palynomorphs (data not shown). Terrestrial palynomorphs occurred as single bisaccate pollen grains only. Structureless organic particles can be either of plant and animal origin. Oxidized residuum was devoid of structureless OM; no other quantitative and/or qualitative differences between samples treated with HNO_3 and those not treated with HNO_3, were observed. Neither dinoflagellate motile stages nor their cysts were found, but some subspherical forms devoid of apertures might be of this affinity (see also Section 4.5.2).

In summary, we observed a strong vertical zonation of microorganisms that is common in

laminated microbial mat ecosystems and results from interactions between the steep physiochemical gradients and physiology of the microorganisms. The colour contrast of the lamination resulted from the different pigment composition of the varied microorganisms comprising the mat, and could thus be used to define layers (Fig. 2). It is assumed, based on previous work (Villanueva et al., 2007) that depth-related differences in structure are more important than diel variations in controlling the distribution of microorganisms.

4.3. Mineralogy of particles within the mat

XRD of 'whole-rock' Qatari mat samples showed that calcite (both low and high Mg calcite), dolomite and aragonite were all present, as well as gypsum, halite and quartz (data not shown). In samples treated with sodium hypochlorite to remove the OM, and washed, similar XRD profiles were obtained, but without the halite. The proportion of each mineral did vary from mat layer to layer, but in most cases the intensity of the 104 dolomite peak was close to that of the main calcite peak (100). The 015* ordering peak of dolomite (2.54A at ca. 35.4^{o}CuKα) did appear to be present in some XRD plots, but was mostly weak or unconvincing, such that the mineral could be a high Mg (50:50) calcite rather than true dolomite (Gregg et al., 2015). Peaks of other minerals could have masked the ordering peaks in some cases.

During the preparation of samples for the identification of the microbes, numerous white 1-5 μm size particles were observed within the mats, along with larger fragments of shell and some quartz grains. Many of the micro-minerals scattered throughout the mat did take on a red colour after Titan Yellow staining. This suggests that high-Mg calcite or dolomite was present. These red grains appeared to be smaller (1 μm size), but more common, in the pink layers, and larger and more obvious in the green/brown layers. These Mg-rich carbonate crystallites occurred within the EPS gelatinous material of the mat, suggesting growth there.

Inorganic carbon isotope data were obtained for 3 samples from the mat and 2 sediment samples from below (Table 1). The $\delta^{13}C$ value for the mat carbonate from the surface layer (0-0.2 cm) was -2.94 ‰, with values for underlying samples from 0.3-0.8 cm and 2-3 cm being -2.04 and -1.93 ‰ respectively. These figures contrast with the $\delta^{13}C$ values of the underlying sediment, +1.61 and 1.49 ‰, which are typical marine values (Tucker and Wright, 1990). The low negative values of the carbonate in the organic-rich mat samples, particularly at the shallowest depth, could indicate microbial involvement in its precipitation, providing ^{12}C-rich HCO_3^-. The $\delta^{18}O$ values for the mat varied from -2.08 at the surface to -0.08 ‰ at 1-2 cm, contrasting with 0.54 and 1.01 ‰ in the sediment below. These differences likely reflect differences in water salinity and temperature (Fig. 3a).

SEM observation of mineral material extracted from mat layers and deposited from suspension on to glass showed an abundance of spheroids in several layers. These structures are subspherical to elliptical, mostly in the range 2-5 μm, with smooth outer surfaces (Fig. 4a,b). Some structures appeared to have amalgamated, and others occurred in clusters or aggregates. These spheroids are strikingly similar to the 'micropearls' reported from Lake Geneva (Jaquet et al., 2013), which are associated with EPS and picoplankton, including *Synechococcus*. Other structures were elongate nested collections of hemispheres, creating curious worm-like objects (Fig. 4c); these were probably permineralised halophilic bacteria. Dumbbell structures were observed, up to 10 μm in length, occurring as individuals or again in clusters (Fig. 4d). There are individual crystals, crystallite clusters, and crystal aggregates. EDS revealed the presence of Ca^{2+} and Mg^{2+}, but usually with Ca^{2+} in excess.

4.4. Elemental analyses

TOC, TN, TS and TP contents in the Mesaieed mat sample are shown in Fig. 5 and Table S1. TOC content was highest (9.8 %) in the surface layer and ranged between 8.6 and 9.6 % in the upper 2 cm of the mat. TOC decreased to 4.6 % in the underlying darker layer (2-3 cm), though this was still significantly elevated compared with the TOC content of the carbonate mud (ca. 1 %) beneath the mat. In a similar manner, TS (0.1 – 1.1 %) and TN (0 – 1.2 %) were highest in the surficial layer, and decreased with depth. However, the decline within the upper 2 cm was much more marked, in particular for TS content, which decreased to less than half that of the surface layer by 8 mm depth. TP ranged from 0.25 to 0.5 % and was lowest in the surface layer, and highest just 1 mm below this, and then declined to 1 cm depth. Below 1 cm and down to the bottom of the mat TP was relatively constant. C/N ratios ranged from 7.7 to 9.3, with an overall increase with depth in the upper 2 cm of the mat. Within the darker layer at 3-4 cm, it was significantly higher (14.6), almost 2x that at the surface. In the underlying sediment TN was below the limit of detection (0.1 %), so the ratio could not be derived, but must have been >10.

4.5. Biomarker characterization and inferred sources

The specific microbial communities in the different layers of a microbial mat give rise to differences in lipid biomarker distribution (e.g. Boon et al., 1983; Boudou et al., 1986a,b; Grimalt et al., 1992; Zeng et al., 1992; Bühring et al., 2009; Sherf and Rullkötter, 2009; Nitti et al., 2012; Pagès et al., 2014; Blumenberg et al., 2015). Lipid biomarkers were analysed for 5 out of the 7 sampled mat layers (Fig. 2): the oxic photosynthetic surface layer (0-0.2 cm depth), the light brown layer (0.3-0.8 cm depth) containing sulphur-oxidising bacteria and Alphaproteobacteria, the distinct opaque layer immediately below this (0.8-1 cm depth) containing a mix of *Lyngbya, Thiocapsa,* and *Beggiatoa*, the pale brown layer (1-2 cm depth) containing *Beggiatoa*, the dark-brown layer (2-3 cm) containing Deltaproteobacteria, halophilic bacteria and the cyanobacterium *Synechococcus*, and finally the dark layer (3-4 cm) containing Deltaproteobacteria, halophilic bacteria, *Lyngbya,* and *Thiocapsa*.

Hydrocarbons found in the neutral apolar fraction included *n*-alkanes, *n*-alkenes and isoprenoids (Fig. 5). The major compounds in the neutral polar fraction included sterols and stanols, represented predominantly by dinosterol and the C_{27} and C_{29} 4-desmethyl sterols, as well as hopanoids. Over 30 total fatty acyl structures were also detected in the PL, GL and free FA forms; the former were the most abundant but all three fractions had similar distributions. Additional bacterial lipids included DAGEs and branched GDGTs (*br*GDGTs)-Ia to -IIIa (Schouten et al., 2013). Dominant archaeal lipids were represented by 2,3-di-*O*-phytanylglycerol (archaeol) and isoprenoid GDGTs (*i*GDGTs)-0 to -4 (Schouten et al., 2013).

4.5.1. Alkanes, alkenes and isoprenoids

n-Alkanes, *n*-alkenes and isoprenoid hydrocarbons were detected in four layers (Fig. 6, Table 2). The *n*-alkenes ranged from C_{17}-C_{21}, contained one or two double bonds and were not detected below 0.8 cm. The *n*-alkanes ranged from C_{16} to C_{31} (Fig. 6) and total concentrations ranged from 4 µg/g TOC (1-2 cm) to 16.7 µg/g TOC (0.8-1.0 cm). They were dominated in the surficial layer by *n*-C_{17} (81% of total *n*-alkanes), a known cyanobacterial biomarker (Han et al., 1968), which has also been identified in hypersaline microbial mats (Grimalt et al., 1992; Fourçans et al., 2004; Rontani and Volkman, 2005; Wieland et al., 2008; Sherf and Rullkötter, 2009).

The concentrations and relative abundances of high molecular weight (HMW) *n*-alkanes (C_{22} to C_{31}) were lowest at the surface and increased with depth to a maximum at 0.8-1 cm (14.05 µg/g TOC) but decreased at 1-2 cm (3.1 µg/g TOC) and were not detected in the deepest samples below 3 cm. The series could be further characterized by the carbon preference index (CPI), reflecting the ratio of odd/even *n*-alkanes:

$$CPI = (C_{23} + C_{25} + C_{27} + C_{29} + C_{31})/(C_{24} + C_{26} + C_{28} + C_{30})$$

CPI ranged from 0.5, with a maximum of 1.7 occurring at 0.3-0.8 cm.

Boudou et al. (1986a,b) noted for Polynesian microbial mats in shallow lagoonal ponds that hydrocarbon concentration (4.7 to 7.5 µg/g TOC) was higher in the anaerobic than in the top cyanobacterial layers. However, their reported values are much lower than ours. The low CPI values of the HMW *n*-alkanes suggest that they were not derived from leaf wax, except perhaps in part at 0.3 to 0.8 cm depth, but instead could be related to diagenetic processes (Eglinton et al., 1962; Clark and Blumer, 1967) or allochthonous inputs of degraded OM, either petroleum contamination, weathered kerogen or highly degraded soil.

Isoprenoid hydrocarbons were abundant in all horizons and included phytane, phytene, phytadienes and squalene (Fig. 6), the last being discussed in Section 4.5.7. Phytane accounted for 0.01-2.7 µg/g TOC with the highest concentration at 0.3-0.8 cm. Phytene dominated the hydrocarbon profile at the surface, with concentration ranging from 0.1 µg/g TOC, with a maximum of 11.2 µg/g TOC at 0-0.2 cm.

Abundant phytane has also been reported in the deepest layers of a Kiritimati hypersaline microbial mat (Bühring et al., 2009). It is thought to be primarily derived from the phytyl side chain of chlorophyll *a* or bacteriochlorophyll of phototrophic organisms (Volkman and Maxwell, 1986). However, other possible sources include lipids of methanogenic (e.g. Langworthy et al., 1982; Volkman, 1986; Rowland, 1990) and halophilic Archaea (Kates et al., 1965; Nissenbaum et al., 1972; Anderson et al., 1977).

The rapid formation followed by decreasing concentration of phytene and phytadiene with depth could be due to either the changing source of OM and/or degradation of phytol. Rontani and Volkman (2005) also attributed the formation of phytene isomers in the coastal hypersaline mats of Camargue to the biodegradation of phytol by sulphate-reducers. Similarly, Bühring et al. (2009) reported a high abundance of phytene in deeper layers of a Kiritimati hypersaline microbial mat and interpreted it as a diagenetic product of the phytol side chain of chlorophyll or bacteriochlorophyll (Volkman and Maxwell, 1986).

No highly branched isoprenoid alkenes (HBIs) characteristic of diatoms (C_{20}, C_{25} and C_{30}) were found, although C_{20}, C_{21} and C_{22} HBIs have been reported in Abu Dhabi microbial mats (Kenig et al., 1990; Sinninghe Damsté et al., 2005).

4.5.2. Steroids

Fig. 7 shows a partial ion current chromatogram of the polar fraction for the 0.8-1.0 cm layer from the Qatar intertidal microbial mat, showing the range of hopanols, sterols and also *n*-alkanols. 4α,23,24-Trimethyl-5α-cholest-22E-en-3β-ol (dinosterol) was one of the most abundant compounds and predominant among the stanols and sterols (Table 2). The concentrations of total 4-desmethyl C_{27-29} sterols decreased within the first mm of the mat but remained rather constant in deeper layers; stanol concentrations were more variable with a

peak at 2-3 cm. These profiles differed that of dinosterol (0.4-13 μg/g TOC), which was relatively high throughout the mat except at 1-2 cm (0.4 μg/g TOC; Fig. 7a).

It is very likely that marine organisms (algal phytoplankton) are the major contributors of C_{27-29} sterols and stanols to the mats. This is confirmed by abundant dinosterol and 4α,23,24-trimethyl-5α-cholestan-3β-ol (dinostanol), both of which are produced almost exclusively by dinoflagellates (Robinson et al., 1984; Volkman et al., 1999). A high concentration of dinosterol may be related to periodically increased productivity of marine algae during red tides, which are common in the Arabian Gulf (Richlen et al., 2009). The dinoflagellate responsible for red blooms in the Arabian Gulf is *Cochlodinium polykrikoides* (Richlen et al., 2009, Hamzehei et al., 2013) belonging to the family *Gymnodiniaceae,* comprising three red tide producing genera - *Cochlodinium*, *Gymnodinium* and *Gyrodinium*. Pirretti et al. (1997) reported the presence of dinosterol and dinostanol in *Gymnodinium* and it is possible that *Cochlodinium* can also biosynthesize dinosterol and dinostanol and serve as their source in Mesaieed mats. However, neither motile nor cyst stages of these species were found (data not shown). Lack of dinoflagellates in the Mesaieed mats could indicate that these forms, if present during their accumulation, underwent subsequent bacterial decay, presumably during early diagenesis. Theca of dinoflagellate motile stages are built of cellulose, which is readily biodegradable. Cyst stages, particularly hypnozygotic resting cysts, in many species are comprised of much more resistant biopolymer, dinosporin, the reason that cysts are so well preserved as fossils (most fossil dinoflagellate cysts are hypnozygotic cysts). However, a majority of modern dinoflagellate species produce non-fossizable cysts and only 13-16 % have resting cysts (e.g. Head, 1996 and references therein).

4.5.3. Alcohols

C_{18}-C_{30} *n*-alkanols were detected in the polar fraction (Fig. 7). They were most abundant in the surface layer (Fig. 8b) with C_{28} being the dominant homologue (Fig. 7). Nichols and Jones (1985) reported HMW alcohols in tropical seagrass, and given the wide presence of seagrass leaves in the mat we assign the C_{22}-C_{30} *n*-alkanols to them. Interestingly, HMW *n*-alkanol concentrations tracked those of HMW *n*-alkanes (Fig. 8b), suggesting a similar source (see Section 5).

4.5.4. FAs

The distributions of PLFAs, GLFAs and the free fatty acids FAs (FFAs) strongly resembled each other, although the first contained the greatest variety. Overall, the FFAs made up a minor portion of total FAs, which are instead dominated by components in the PLFA and GLFA fractions. The total concentration of FAs was highest in the surface layer of the mat and generally decreased with depth to uniformly low values below 1.0 cm (Fig. 7c-e). In contrast, hydroxy (α-OH, C_{16}-C_{26} and β-OH, C_{14}-C_{18}) FAs were most abundant in the deepest layers of the mat.

The PLFA distribution was the most complex, comprising 32 saturated, branched, and monounsaturated components, ranging from C_{14}-C_{28}. Saturated and monounsaturated FAs were predominant, whereas branched FAs were least abundant (Fig. 7c-e). *n*-Hexadecanoic acid was dominant in all of the samples and fractions, typically followed by a C_{18} monounsaturated FA. The *iso* and *anteiso* acids possibly derive from gram-positive and sulphate-reducing bacteria in the mats (Grimalt et al., 1992; Findlay and Dobbs, 1993), consistent with our optical identification. α-OH FAs have been reported in many bacteria, protozoa and yeasts (Zelles et al., 1995). β-OH FAs are associated with the

lipopolysaccharides of gram-negative bacteria, but can also be present as the fatty acyl components of phospholipid FAs (Zelles, 1997).

4.5.5. Hopanoids

Hopanoids were detected in the apolar, neutral polar, phospholipid and glycolipid fractions, although we note that additional hopanoids likely occurred as bacteriohopanepolyols (BHPs), which were not analysed. In the apolar fraction, hopanoids were represented by diploptene [hop-22(29)-ene] and minor hopenes. The concentration of diploptene generally increased with depth, reaching a maximum of 6.1 μg/g TOC at 0.8-1 cm, before decreasing somewhat at 2-3 cm (Fig. 8f, Table 2). It occurs in a range of bacteria (Rohmer et al., 1984; Jahnke et al., 2004).

Hopanols (C_{30-32}, with C_{31} and C_{32} dominant) and an unidentified hopanoid, the most abundant of all compounds, occurred in the neutral polar fraction (Fig. 7, 8f). The concentration of hopanols also increased with depth, reaching a maximum of 2.4 μg/g TOC at 0.8-1 cm (Fig. 8f, Table 2), whereas an unknown hopanoid was detected at 0.8-3 cm. The increase in hopanol and diploptene concentration with depth likely arises from the bacterial community changes, with bacteria in the subsurface layers producing more hopanols than surface-dominating cyanobacteria.

Bishomohopanoic acid (17β,21β; C_{32}) occurred in the free acid fraction and was liberated via hydrolysis of the phospholipid and glycolipid fractions. In all fractions it only occurred in the deepest dark-brown anoxic layers (2-4 cm) and we attribute it to Deltaproteobacteria thriving at this depth or diagenetic degradation of BHPs.

4.5.6. DAGEs

Two non-isoprenoid DAGEs (C_{15}/C_{16} and C_{16}/C_{17} branched alkyl components) were detected in the phospholipid and neutral polar fractions. In the latter fraction, however, structural assignment was tentative due to co-elution with other compounds. Interestingly, both DAGEs occurred at 2-4 cm, i.e. in the darkest and deepest mat layers (Fig. 8f). Non-isoprenoid DAGEs have been detected in hydrothermal environments (Zeng et al., 1992; Jahnke et al., 2001; Pancost et al., 2005, 2006; Bradley et al., 2009; Kaur et al., 2011; Hamilton-Brehm et al., 2013), upper Pliocene iron sulphide nodules (van Dongen et al., 2007), and diverse marine sediments (Hinrichs et al., 2000; Pancost et al., 2001; Blumenberg et al., 2004; Arning et al., 2008; Hernandez-Sanchez et al., 2014). Here, given that the peak concentration of DAGEs corresponded to the presence of sulphate-reducing bacteria, we suggest that these are the source, as has been inferred in settings dominated by anaerobic oxidation of methane (Hinrichs et al., 2000; Pancost et al., 2001; Blumenberg et al., 2004), and consistent with their recent identification in a mesophilic strain of Deltaproteobacteria (Grossi et al., 2015, Vinçon-Laugier et al., 2016).

4.5.7. Archaeol and squalene

Archaeol was detected in most layers of the Mesaieed mat (Fig. 8g); it is a DAGE comprising two C_{20} isoprenoid alkyl chains, and is derived from, and widespread in, Archaea (DeRosa and Gambacorta, 1988). As such, it has been found in diverse settings, including geothermal sinters (Pancost et al., 2005, 2006; Kaur et al., 2015), microbial mats (Bühring et al., 2009), hypersaline settings (Jahnke et al., 2008; Bray et al., 2012), cold seep sediments

(e.g. Hinrichs et al., 2000; Pancost et al., 2001; Zhang et al., 2003) and peats (Pancost et al., 2011; Zheng et al., 2014). In the Mesaieed mat, the concentration was highly variable with depth, ranging from 0.004 μg/g TOC to 0.48 μg/g TOC. Although it is commonly suggested to be derived from methanogens (Weijers et al., 2004; Pancost et al., 2011), its widespread phylogenetic occurrence dictates caution in this interpretation. In general, archaeol concentrations are low and then increase in the deepest mat layer.

Squalene was detected in all mat layers and is among the most abundant hydrocarbons in several. It is commonly invoked as an archaeal lipid (Holzer et al., 1979; Tornabene et al., 1979; Brassell et al., 1981). However, it is also a precursor of triterpenoid biosynthesis and commonly reported in cyanobacterial mats (Boon et al., 1983; Dobson et al., 1988; Rontani and Volkman, 2005; Sherf and Rullkötter, 2009; Allen et al., 2010) and cultures (Gelpi et al., 1970). In the Mesaieed mat, its concentration depth profile (Fig. 8g), increasing with depth within the upper part of the mat, reaching 6.4 μg/g TOC at 0.8-1 cm and then rapidly decreasing in deeper mat layers, being undetected below 2 cm, parallels those of neither archaeal nor bacterial lipids suggesting a complex, potentially mixed source.

4.5.8. GDGTs

GDGTs, released by acid hydrolysis of the glycolipid and phospholipid fractions, were present in all layers (Fig. 9). The dominant GDGTs were the branched components Ia, IIa and IIIa (Fig. 9). The abundance of branched GDGTs was slightly variable from layer to layer but generally was highest at 0.8-1 cm.

The dominance of branched GDGTs suggests a substantial allochthonous terrestrial component. Alternatively, GDGT-Ia-IIIa derive from the mat-forming bacteria, possibly from anaerobic *Acidobacteria* indigenous to the mats (Weijers et al., 2009, 2010; Sinninghe Damsté et al., 2011). This is consistent with in situ production of branched GDGTs in other marine sediments (e.g. Zhu et al., 2013), and hot spring settings (Hedlund et al., 2013; Zhang et al., 2013).

The isoprenoid GDGT distributions are unusual for marine sediments (i.e. Schouten et al., 2013), suggesting that some or all were produced within the mat. GDGT-0 occurred in all horizons and its concentration was particularly high at the bottom of the mat. Isoprenoid GDGTs-1-3 exhibited similar depth profiles, with significantly higher concentration at 4 cm. Crenarchaeol, bearing a cyclohexyl moiety in addition to four cyclopentyl rings and derived predominantly or exclusively from *Thaumarchaeota* (Schouten et al. 2013), was absent from the top layer (0-0.2 cm) and most abundant at 0.8-1 cm.

The high abundance of GDGT-0 (the highest in the bottom layer) and the presence of crenarchaeol suggest GDGT sources from methanogens and *Thaumarchaeota*, respectively. Crenarchaeol has been detected previously in microbial mats (Zhang et al., 2006; Schouten et al., 2007) and could derive from either in situ organisms or allochthonous inputs of marine organisms; its absence in the top layer suggests the former. Although GDGT-0 is widespread in Archaea (Schouten et al., 2013) it likely derives from methanogens, especially in the lower layer, where its abundance is particularly high. The *i*GDGT-1-3 compounds could derive from a range of sources, but we exclude allochthonous *Thaumarchaeota* because the abundance of these GDGTs is much higher than that of crenarchaeol.

5. An integrated perspective on mat formation and diagenetic processes

The composition of mat species and the biogeochemical processes occurring in mats vary

in response to changes in salinity, water cover, light intensity and temperature (e.g. Jørgensen et al., 1979; Revsbech et al., 1983; Canfield and Des Marais, 1993; Denich et al., 2003; Des Marais, 2003). It is probable that the dominant controls on the development of the Mesaieed mat in this setting were deposition and remobilization of sediments which determine the micro-bathymetry within the lagoon, as well as the morphology of the chenier beach and breaches in this barrier. These factors influence the frequency and depth of tidal flooding and the degree of restriction, and therefore salinity and temperature, all important factors controlling biomass productivity and ecology of the mat.

5.1. Surficial layer

The surficial layer (0-0.2 cm depth) is dominated by heterotrophic cyanobacteria, Proteobacteria, Halobacteria, high porewater O_2, salinity and alkalinity, and high TOC content. Consistent with a dominance of cyanobacteria were high concentrations of phytene and *n*-heptadecane. Concentrations of FAs in all fractions (and crucially, PLFAs) were also highest in the surface horizon, suggesting that total bacterial biomass was also highest and declines or degrades with depth. Sterol concentrations were also highest, suggesting strong allochthonous inputs; high C/N values suggest that some of these could be from terrigenous plants or seagrass (Table S1). The seagrass source of OM is also suggested by the highest concentrations of HMW *n*-alkanols in this layer. Both the $\delta^{13}C$ and $\delta^{18}O$ values of the carbonate precipitates in the mat were low compared with typical marine values and more negative than the carbonate sediment underlying the mat (Table 1). These observations are attributed to a strong microbial involvement in carbonate precipitation, and the relatively high temperature of pore fluid, respectively.

5.2. Sub-surficial layers

A decline in microbial biomarkers, especially fatty acids, occurred at 0.2-0.3 cm depth, with many biomarker concentrations being below the detection limit. With the rapid consumption of dissolved oxygen in porewaters, anaerobic purple sulphur bacteria were most abundant. Therefore, this depth apparently marks the transition from photosynthesis to heterotrophy and an enhanced S cycle, represented by decreasing cyanobacteria and the occurrence of purple sulphur bacteria and *Beggiatoa*.

In general, deeper layers 0.3 to 2 cm, are associated with highly variable biomarker abundances, which we attribute to a combination of factors but predominantly to pulses of allochthonous inputs of organic matter into a mat being progressively degraded by heterotrophic processes. The latter was reflected by the ongoing decrease in fatty acid concentrations through these horizons as well as the steady increase in $_PCO_2$, likely due to respiration, and an associated decrease in carbonate mineral SIs (Fig. 3).

At 0.3 to 0.8 cm and 1-2 cm depth, the concentrations of hopanoids, stanols *n*-alkanes, *n*-alkanols, and squalene were all relatively high, and CPIs were the highest for the entire mat; dinosterol and *n*-alkyl lipids were particularly abundant in the 1-2 cm horizon (Fig. 8). Overall, this suggests relatively fresh and abundant OM derived from both microorganisms and especially allochthonous inputs. Consistent with this, the layers were populated by sulphur-oxidizing and purple non-sulphur bacteria, as well as abundant seagrass remains. (Fig. 8b), perhaps suggesting a seagrass source.

The mat composition was significantly different at 0.8-1 cm. This portion of the mat was dominated by a mix of cyanobacteria (which have either migrated down within the mat or are

reworked or buried dead cells), purple sulphur bacteria, sulphur-oxidising bacteria, and dinoflagellates (Fig. 2, Table 2). Consistent with this, the horizon was characterised by abundant bacterial biomarkers (hopanols, hopanes, hopenes and an unknown hopanoid), squalene and crenarchaeol, as well as allochthonous biomarkers, including both GDGT-Ia-IIIa, dinosterol and *n*-alkyl lipids. However, ongoing diagenetic degradation resulted in lower concentrations of chlorophyll-derived isoprenoids and sterols (other than dinosterol). C/N ratios were also elevated; although this could be related to seagrass inputs, visual analyses suggest that these were lower in this horizon. An increase in C/N ratios was also observed by Wieland et al. (2008) in a Salin-de-Giraud hypersaline mat; this could be the result of an increasing contribution of high carbon content bacterial cell remains and EPS (amorphous organic matter) that tend be buried and preferentially preserved.

In these horizons, the biomarker distribution also records more nuanced aspects of OM degradation. These layers were characterised by the highest (but variable) concentrations of hopanoids (Fig. 8f, Table 2), which could partly reflect their formation from more complex BHPs. Although sterol concentrations were low, stanol to sterol ratios were high (Table 2, Fig. 8a), perhaps reflecting their formation via reduction (Wakeham, 1989 and references therein).

Crucially, the chemical and mineralogical features of this horizon appear to have been dominated by diagenetic processes. Salinity, temperature and saturation indices of all carbonate minerals and gypsum further decreased through this interval (Fig. 3a,b), but dolomite remained supersaturated (SI ca. 2). This is consistent with the occurrence of spheroids, dumbbells and crystallites (Fig. 4) composed of calcium carbonate with variable magnesium. Moreover, their close association with the gelatinous EPS suggests that the precipitation of carbonate (and possibly dolomite) was mediated by microorganisms, which in some cases may have been permineralised (Jaquet et al., 2013; Paulo and Dittrich, 2013; Bontognali et al., 2014).

5.3. Deepest mat layers

The deepest layers of the mat (2-5 cm) were characterised by a near complete consumption of O_2 via the degradation of OM, with the latter reflected in the continued decline in TOC content and FA concentrations. Consistent with this, these layers were dominated by anaerobic heterotrophs (Fig. 2). The presence of cyanobacteria at this depth (Fig. 2) suggests that this deeper mat material included altered old OM that was originally the same as at the top of the mat, but the very low abundance of associated biomarkers (i.e. phytenes, FAs) confirms that much of this primary OM had been remineralised. Interestingly, C_{15}/C_{16}, C_{16}/C_{17} DAGEs and homohopanoic acids occurred only in this layer (Fig. 8f) and were potentially derived from the sulphate-reducing bacteria (Deltaproteobacteria). Archaeal lipids, archaeol and GDGT-0, were also most abundant at 2-3 cm depth (Fig. 8g, 9) suggesting that at least some OM degradation occurs via methanogenesis. Intriguingly, some biomarker diagenetic products, including geohopanoids and *n*-alkanes were less abundant than in the overlying layer, perhaps indicating that the concentration was diluted by mixing of mat OM with the underlying substrate. Salinity, pH, and temperature decreased with depth, and the high $_{P}CO_2$ limited the potential for carbonate precipitation. Nonetheless, carbonate was still present and low negative $\delta^{13}C$ values indicate a continuing microbial involvement in precipitation. Carbonate $\delta^{18}O$ values were less negative than nearer the surface, possibly due to precipitation from water with a lower temperature.

5.4. Overview

Overall, mats in these settings appear to represent a significant but spatially heterogeneous accumulation of bacterial OM, driven in the case of the Mesaieed mat by bacterial photosynthetic processes. However, this OM appears to be rapidly altered and degraded. The mat is also characterised by abundant allochthonous seagrass, algal and dinoflagellate inputs, but these appear to be concentrated in only some horizons, suggesting an episodic nature to their inputs, perhaps via algal blooms in the case of dinoflagellates and rainfall events in the case of seagrass. The relatively small pool of hydrocarbons (37-69 $\mu g\ g^{-1}$ TOC per layer) and high degree of OM degradation suggest very low OM preservation potential of these mesohaline mats in the Arabian Gulf, even though the initial bioproductivity is high.

Crucially, biological processes exert a strong control on the carbonate geochemistry of mats. Photosynthesis in the shallowest layers removes CO_2 resulting in supersaturation with respect to both calcium carbonate and dolomite. This drives the precipitation of perhaps both carbonate minerals. It is possible that in more mature mats, such precipitates could protect co-occurring OM from further degradation and could facilitate its preservation (Bontognali et al., 2010). It is suggested that in some situations early carbonate precipitation within an intertidal meso- hyper- saline microbial mat will lead to preservation of OM and so contribute to the formation of source rocks in evaporitic environments. We also suggest that other proposed scenarios for OM preservation, including sabkha progradation burying organic-rich tidal-flat-lagoonal facies, lagoonal lime muds rapidly transgressing over organic-rich tidal-flat sediments, or whitings (Kendall and Alsharhan, 2012) are important explanations for the formation of source rocks in such settings.

6. Conclusions

The microbial composition of Mesaieed mesohaline microbial mats has been inferred from a combination of optical microscopic, previously published genetic analyses on related mats and lipid biomarker abundances. The mat biomass is composed predominantly of cyanobacteria, purple sulphur and purple non-sulphur bacteria, halophilic bacteria, and sulphate-reducing bacteria, consistent with a diverse suite of bacterial lipids (phytene, hopanoids, FAs, DAGEs, and *br*GDGTs). Biomarkers reveal other microbial inputs, particularly *Thaumarchaeota* and methanogens (*i*GDGTs, archaeol). Allochthonous biomass components are represented by *Halodule* seagrass, dinoflagellate (and other algal) biomarkers and perhaps *br*GDGTs and HMW *n*-alkyl lipids. All data reveal that the Mesaieed mat is characterised by photoautotrophy in the upper layers, anaerobic heterotrophy (especially sulphate reduction) in underlying layers and methanogenesis in the deepest layers (below 3 cm). The mat profiles also provide insight into early diagenetic processes associated with the degradation of OM by sulphate reduction and methanogenesis. This includes loss of TOC, an increase in C/N ratios due to selective preservation of EPS, alteration of biomarkers (i.e. sterols to stanols), and the precipitation of Mg-rich carbonates. Crucially, the Mesaieed mat is evidently characterised by rapid degradation of OM resulting in a very low contribution of OM, indicating that additional processes, such as mineral precipitation or burial by lime mud in the Arabian Gulf, are crucial to ensuring the preservation of OM – and by extension the formation of hydrocarbon deposits.

Acknowledgements

We are indebted to two anonymous reviewers for their constructive and helpful comments and to J. Maxwell and B. van Dongen for editorial handling, all of which significantly improved this paper. We thank the Mesaieed Port Authority for permission to collect mats and J. Jameson and C. Strohmenger (Exxon Mobil Qatar Centre for Coastal Research) for introducing us to the area. We are indebted to S. Mey Didi-Ooi, G. Tong and J. Simmonds for field assistance and collection of some data. A. Gąsiewicz (Polish Geological Institute) is thanked for encouragement and suggestions. We thank D. Davies (School of Chemistry, University of Bristol) for elemental, H. Sparkes and I. Hill (School of Chemistry, University of Bristol) for XRD, S. Davies and J. Jones (School of Chemistry, University of Bristol) and L. Bowen (Durham University) for SEM, and I. Boomer (University of Birmingham) for isotopic analyses. J. Williams, A. Kuhl, and I. Bull (School of Chemistry, University of Bristol) are thanked for help with instruments. We also wish to thank the Natural Environment Research Council (NERC) for partial funding of the mass spectrometry facilities at Bristol (contract no. R8/H10/63). M.S. was supported by a Mobility Plus programme postdoctoral fellowship of the Ministry of Science and Higher Education of Poland. R.D.P. acknowledges the Royal Society Wolfson Research Merit Award.

References

Al-Thani, R., Al-Najjar, M.A.A., Al-Raei, A.M., Ferdelman, T., Thang, N.M., Al Shaikh, I., Al-Ansi, M., de Beer, D., 2014. Community structure and activity of a highly dynamic and nutrient-limited hypersaline microbial mat in Um Alhool Sabkha, Qatar. PLoS ONE 9, e92405.

Allen, M.A., Neilan, B.A., Burns, B.P., Jahnke, L.L., Summons, R.E., 2010. Lipid biomarkers in Hamelin Pool microbial mats and stromatolites. Organic Geochemistry 41, 1207-1218.

Alsharhan, A.S., Kendall, C.G.St.C., 2003. Holocene coastal carbonates and evaporites of the Southern Arabian Gulf and their ancient analogues. Earth Science Reviews 61, 191-243.

Anderson R., Kates, M., Baedecker, M.J., Kaplan, I.R., Ackman, R.G., 1977. The stereoisomeric composition of phytanyl chains in lipids of Dead Sea sediments. Geochimica et Cosmochimica Acta 41, 1381-1390.

Arning, E.T., Birgel, D., Schulz-Vogt, H.N., Holmkvist, L., Jørgensen, B.B., Larson, A., Peckmann, J., 2008. Lipid biomarker patterns of phosphogenic sediments from upwelling regions. Geomicrobiology Journal 25, 69–82.

Balskus, E.P., Case, R.J., Walsh, C.T., 2011. The biosynthesis of cyanobacterial sunscreen scytonemin in intertidal microbial mat communities. FEMS Microbiology Ecology 77, 322-332.

Baltzer, F., Kenig, F., Boichard, R., Plaziat, J.-C., Purser, B.H., 1994. Organic matter distribution, water circulation and dolomitization beneath the Abu Dhabi Sabkha (United Arab Emirates). In: Purser B., Tucker M., Zenger D. (Eds), Dolomites. A Volume in Honour of Dolomieu. IAS Special Publication 21, 409-427.

Becraft, E.D., Cohan, F.M., Kuhl, M., Jensen, S.I., Ward, D.M., 2011. Fine-scale distribution patterns of Synechococcus ecological diversity in microbial mats of Mushroom Spring, Yellowstone National Park. Applied and Environmental Microbiology 77, 7689-7697.

Berg, J.S., Schwedt, A., Kreutzmann, A., Kuypers, M.M.M., Milucka, J., 2014. Polysulfides as intermediates in the oxidation of sulfide to sulfate by *Beggiatoa* spp. Applied and Environmental Microbiology 80, 629-636.

Blumenberg, M., Seifert, R., Reitner, J., Pape, T., Michaelis, W., 2004. Membrane lipid patterns typify anaerobic methanotrophic consortia. Proceedings of the National Academy of Science USA 101, 11111-11116.

Blumenberg, M., Thiel, V., Reitner, J., 2015. Organic matter preservation in the carbonate matrix of a

recent microbial mat – Is there a 'mat seal effect'? Organic Geochemistry 87, 25-34.

Bontognali, T.R.R., Vasconcelos, C.G., Warthmann, R., Bernasconi, S.M., Dupraz, C., Strohmenger, C.J., McKenzie, J.A., 2010. Dolomite formation within microbial mats in the coastal sabkha of Abu Dhabi (United Arab Emirates). Sedimentology 57, 824–844.

Bontognali, T.R.R., McKenzie, J.A., Warthmann, R.J., Vasconcelos, C., 2014. Microbially influenced formation of Mg-calcite and Ca-dolomite in the presence of exopolymeric substances produced by sulphate-reducing bacteria. Terra Nova 26, 72-77.

Boon, J.J., Hines, H., Burlingame, A.L., Klok, J., Rijpstra, W.I.C., de Leeuw, J.W., Edmunds, K.E., Eglinton, G., 1983. Organic geochemical studies of Solar Lake laminated cyanobacterial mats. In: Bjorøy, M., Albrecht, P., Cornford, C., de Groot, K., Eglinton, G., Galimov, E., Leythaeuser, D., Pelet, R., Rullkötter, J., Speers, G. (Eds), Advances in Organic Geochemistry 1981. John Wiley & Sons, New York, pp. 207-227.

Boudou, J.P., Trichet, J., Robinson, N., Brassell, S.C., 1986a. Profile of aliphatic hydrocarbons in a recent Polynesian microbial mat. International Journal of Environmental Analytical Chemistry 26, 137-155.

Boudou, J.P., Trichet, J., Robinson, N., Brassell, S.C., 1986b. Lipid composition of a recent Polynesian microbial mat sequence. Organic Geochemistry 10, 705-709.

Bradley, A., Fredricks, H., Hinrichs, K.-U., Summons, R.E., 2009. Structural diversity of diether lipids in carbonate chimneys at the Lost City Hydrothermal Field. Organic Geochemistry 40, 1169–1178.

Brassell, S.C., Wardroper, A.M.K., Thomson, I.D., Maxwell, J.R., Eglinton, G., 1981. Specific acyclic isoprenoids as biological markers of methanogenic bacteria in marine sediments. Nature 290, 693-696.

Bray, P.S., Jones, C.M., Fallon, S.J., Brocks, J.J., George, S.C., 2012. Radiocarbon analysis of halophilic microbial lipids from an Australian salt lake. Quaternary Research 77, 104–109.

Bühring, S.I., Smittenberg, R.H., Sachse, D., Lipp, J.S., Golubic, S., Sachs, J.P., Hinrichs, K.-U., Summons, R.E., 2009. A hypersaline microbial mat from the Pacific Atoll Kiritimati: insights into composition and carbon fixation using biomarker analyses and a ^{13}C-labeling approach. Geobiology 7, 308-323.

Canfield, D.E., Des Marais, D.J., 1993. Biogeochemical cycles of carbon, sulfur, and free oxygen in a microbial mat. Geochimica et Cosmochimica Acta 57, 3971-3984.

Choi, Y.J., Lee, S.Y., 2013. Microbial production of short-chain alkanes. Nature 502, 571-574.

Clark, R.C., Blumer, M., 1967. Distribution of *n*-paraffins in marine organisms and sediment. Limnology and Oceanography 12, 79-87.

de Wit, R,, van Boekel, W.H.M., van Gemerden, H., 1988. Growth of the cyanobacterium *Microcoleus chthonoplastes* on sulfide. FEMS Microbiology Ecology 53, 203-209.

Denich, T.J., Beaudette, L.A., Lee, H., Trevors, J.T., 2003. Effect of selected environmental and physico-chemical factors on bacterial cytoplasmic membranes. Journal of Microbiological Methods 52, 149-182.

Des Marais, D.J., 2003. Biogeochemsitry of hypersaline microbial mats illustrates the dynamics of modern microbial ecosystems and the early evolution of the biosphere. Biological Bulletin, 204, 160-167.

Dickson, J.A.D., 1966. Carbonate identification and genesis as revealed by staining. Journal of Sedimentary Petrology 36, 491-505.

Dickson, L., Bull, I.D., Gates, P.J., Evershed, R.P., 2009. A simple modification of a silicic acid lipid fractionation protocol to eliminate free fatty acids from glycolipid and phospholipid fractions. Journal of Microbiological Methods 78, 249–254.

Dobson, G., Ward, D.M., Robinson, N., Eglinton, G., 1988. Biogeochemistry of hot spring environments: extractable lipids of a cyanobacterial mat. Chemical Geology 68, 155-179.

Eglinton, G., Gonzalez, A.G., Hamilton, R.J., Raphael, R.A., 1962. Hydrocarbon constituents of the wax coatings of plant leaves: A taxonomic survey. Phytochemistry 1, 89-102.

Emery, K.O., 1956. Sediments and water of Persian Gulf. AAPG Bulletin 40, 2354-2383.

Evans, G., 1966. The Recent sedimentary facies of the Persian Gulf region. Philosophical Transactions of the Royal Society A259, 291-298.

Farrimond, P., Head, I.M., Innes, H.E., 2000. Environmental influence on the biohopanoid composition of recent sediments. Geochimica et Cosmochimica Acta 64, 2985-2992.

Findlay, R.H., Dobbs, F.C., 1993. Quantitative description of microbial communities using lipid analysis. In*:* Kemp, P.F., Sherr, B.F., Sherr, E.B., Cole, J.J. (Eds), Handbook of Methods in Aquatic Microbial Ecology. Lewis Publishers, Boca Raton, pp. 271–284.

Fofonoff, N.P., 1985. Physical properties of seawater: A new salinity scale and equation of state for seawater. Journal of Geophysical Research 90, 3332-3342.

Fourçans, A., de Oteyza, T.G., Wieland, A., Solé, A., Diestra, E., van Bleijswijk, J., Grimalt, J.O., Kühl, M., Esteve, I., Muyzer, G., Caumette, P., Duran, R., 2004. Characterization of functional bacterial groups in a hypersaline microbial mat community (Salins-de-Giraudd, Camargue, France). FEMS Microbiology Ecology 51, 55-70.

Friedman, G.M., 1959. Identification of carbonate minerals by staining methods. Journal of Sedimentary Petrology 29, 87-97.

Gautier, D.L., Kharaka, Y.K., Surdam, R.C., 1985. Relationship of organic matter and mineral diagenesis. Society for Sedimentary Geology Short Course Notes 17, 279 pp.

Gelpi, E., Schneider, H., Mann, J., Oró, J., 1970. Hydrocarbons of geochemical significance in microscopic algae. Phytochemistry 9, 603-612.

Gregg, J.M., Bish, D.L., Kaczmarek, S.E., Machel, H.G., 2015. Mineralogy, nucleation and growth of dolomite in the laboratory and sedimentary environment: A review. Sedimentology 62, 1749-1769.

Grimalt, J.O., de Wit, R., Teixidor, P., Albaiges, J., 1992. Lipid biogeochemistry of *Phormidium* and *Microcoleus*mats. Organic Geochemistry 19, 509-530.

Grossi, V., Mollex, D., Vinçon-Laugier, A., Hakil, F., Pacton, M., Cravo-Laureau, C., 2015. Mono- and dialkyl glycerol ether lipids in anaerobic bacteria: Biosynthetic insights from the mesophilic sulfate reducer *Desulfatibacillum alkenivorans* PF2803^{T}. Applied and Environmental Microbiology 81, 3157-3168.

Hamilton-Brehm, S.D., Gibson, R.A., Green, S.J., Hopmans, E.C., Schouten, S., van der Meer, M.T.J., Shields, J.P., Sinninghe Damsté, J.S., Elkins, J.G., 2013. *Thermodesulfobacterium geofontis* sp. nov., a hyperthermophilic, sulfate-reducing bacterium isolated from Obsidian Pool, Yellowstone National Park. Extremophiles 17, 251–263.

Hamzehei, S., Bidokhti, A.A., Mortazavi, M.S., Gheiby, A., 2013. Red tide monitoring in the Persian Gulf and Gulf of Oman using MODIS data. Technical Journal of Engineering and Applied Sciences 12, 1100-1107.

Han, J., McCarthy, E.D., Calvin, M., 1968. Hydrocarbon constituents of the blue-green algae *Nostoc muscorum, Anacystis nidulans, Phormidium luridum* and *Chlorogloea fritschii*. Journal of the Chemical Society C: Organic 2782-2791.

Head, M.J., 1996. Modern dinoflagellate cysts and their biological affinities. In: Jansonius, J., McGregor, D.C. (Eds), Palynology: Principles and Applications. American Association of Stratigraphic Palynologists Foundation 3, pp. 1197-1248.

Hedlund, B.P., Paraiso J.J., Williams A.J., Huang Q., Wei Y., Dijkstra P., Hungate, B.A., Dong, H.,

Zhang, C.L., 2013. Wide distribution of autochthonous branched glycerol dialkyl glycerol tetraethers (bGDGTs) in U.S. Great Basin hot springs. Frontiers in Microbiology 4, 222.

Hernandez-Sanchez, M.T., Homoky, W.B., Pancost, R.D., 2014. Occurrence of 1-O-monoalkyl glycerol ether lipids in ocean waters and sediments. Organic Geochemistry 66, 1–13.

Hinrichs, K.-U., Summons, R.E., Orphan, V., Sylva, S.P., Hayes, J.M., 2000. Molecular and isotopic analysis of anaerobic methane-oxidizing communities in marine sediments. Organic Geochemistry 31, 1685-1701.

Huber, R., Rossnagel, P., Woese, C.R., Rachel, R., Langworthy, T.A., Stetter, K.O., 1996. Formation of ammonium from nitrate during chemolithoautotrophic growth of the extremely thermophilic bacterium *Ammonifex degensii* gen. nov. sp. nov. Systematic and Applied Microbiology 19, 40-49.

Holzer, G., Oró, J., Tornabene, T.G., 1979. Gas chromatographic-mass spectrometric analysis of neutral lipids from methanogenic and thermoacidophilic bacteria. Journal of Chromatography 186, 795-809.

Illing, L.V., Wells, A.J., Taylor, J.C.M., 1965. Penecontemporary dolomite in the Persian Gulf. In: Pray, L.C., Murray, R.C. (Eds), Dolomitization and Limestone Diagenesis. Society of Sedimentary Geology Special Publications 13, 89-111.

Jahnke, L.L., Eder, W., Huber, R., Hope, J.M., Hinrichs, K.-U., Hayes, J.M., Des Marais, D.J., Cady, S.L., Summons, R.E., 2001. Signature lipids and stable carbon isotope analyses of Octopus Spring hyperthermophilic communities compared with those of *Aquificales* representatives. Applied and Environmental Microbiology 67, 5179–5189.

Jahnke, L.L., Embaye, T., Hope, J., Turk, K.E., van Zuilen, M., des Marais, D.J., Farmer, J.D., Summons, R.E., 2004. Lipid biomarker and carbon isotopic signatures for stromatolite-forming, microbial mat communities and *Phormidium* cultures from Yellowstone National Park. Geobiology 2, 31-47.

Jahnke, L.L., Orphan, V.J., Embaye, T., Turk, K.A., Kubo, M.D., Summons, R.E., Des Marais, D.J., 2008. Lipid biomarker and phylogenetic analyses to reveal archaeal biodiversity and distribution in hypersaline microbial mat and underlying sediment. Geobiology 6, 394–410.

Jaquet, J.-M., Nirel, P., Martignier, A., 2013. Preliminary investigations on picoplankton-related precipitation of alkaline-earth metal carbonates from meso-oligotrophic lake Geneva (Switzerland). Journal of Limnology 72, 592-605.

Javor, B., Castenholz, R.W., 1981. Laminated microbial mats, laguna Guerrero Negro, Mexico. Geomicrobiology Journal 2, 237-273.

Jørgensen, B.B., Revsbech, N.P., Blackburn, T.H., Cohen, Y., 1979. Diurnal cycle of oxygen and sulfidemicrogradients and microbial photosynthesis in a cyanobacterial mat. Applied Environmental Microbiology 38, 46-58.

Kates, M., Yengoyan, L.S., Sastry, P.S., 1965. A dietheranalog of phosphatidylglycerophosphate in *Halobacteriumcutirubrum*. Biochimica et Biophysica Acta – Lipids and Lipid Metabolism 98, 252-268.

Kaur, G., Mountain, B.W., Hopmans, E.C., Pancost, R.D., 2011. Relationship between lipid distribution and geochemical environment within Champagne Pool, Waitapu, New Zealand. Organic Geochemisty 42, 1203-1215.

Kendall, C.G.St.C., Alsharhan A.S., Cohen A., 2002. The Holocene tidal flat complex of the Arabian Gulf coast of Abu Dhabi. *I*n: Barth, H.-J., Böer, B. (Eds), Sabkha Ecosystems. Kluwer Academic Publishers, pp. 21-35.

Kendall, C.G.St.C., Alsharhan, A.S., 2012. Coastal Holocene carbonates of Abu Dhabi, UAE: depositional setting, sediment distribution, and role of cyanobacteria in micritization. IAS Special Publication 43, 205-220.

Kenig, F., Huc, A.Y., Purser, B.H., Oudin, J.-L., 1990. Sedimentation, distribution and diagenesis of organic matter in a Recent carbonate environment, Abu Dhabi. Organic Geochemistry 16, 735-747.

Langworthy, T.A., Tornabene, T.G., Höltzer, G., 1982. Lipids of Archaebacteria. In: Kandler, O. (Ed), Archaebacteria. Gustav Fischer Verlag, Stuttgart, pp. 228-244.

Langworthy, T.A., Holzer, G., Zeikus, J.G., Tornabene, T.G., 1983. Iso- and anteiso-branched glycerol diethers of the thermophilic anaerobe *Thermodesulfotobacterium commune*. Systematic and Applied Microbiology 4, 18-26.

Lindholm, R.C., Finkelman, R.B., 1972. Calcite staining: semiquantitative determination of ferrous iron. Journal of Sedimentary Petrology 42, 239-242.

Lloyd, J.W., Pike, J.G., Eccleston, B.L., Chidley, T.R.E., 1987. The hydrogeology of complex lens conditions in Qatar. Journal of Hydrology 89, 239-258.

Madkour, F.F., Gaballah, M.M., 2012. Phytoplankton assemblage of a solar saltern in Port Fouad, Eygpt. Oceanologia 54, 687-700.

Martínez-Alonso, M., Mir, J., Caumette, P., Gaju, N., Guerrero, R., Estevem I., 2004. Distribution of phototrophic populations and primary production in a microbial mat from the Ebro Delta, Spain. International Microbiology 7, 19–25.

Nissenbaum, A., Baedecker, M.J., Kaplan, I.R., 1972. Organic geochemistry of Dead Sea sediments. Geochimica et Cosmochimica Acta 36, 709-727.

Nitti, A., Daniels, C.A., Siefert, J., Souza, V., Hollander, D., Breitbart, M., 2012. Spatially resolved genomic, stable isotopic, and lipid analyses of a modern freshwater microbialite from Cuatro Ciénegas, Mexico. Astrobiology 12, 685-698.

Omoregie, E.O., Crumbliss, L.L., Bebout, B.M., Zehr, J.P., 2004. Comparison of diazotroph community structure in *Lyngbya* sp. and *Microcoleus chthonoplastes* dominated microbial mats from Guerrero Negro, Baja, Mexico. FEMS Microbiology Ecology 47, 305-318.

Pagès, A., Grice, K., Ertefai, T., Skrzypek, G., Jahnert, R., Greenwood, P., 2014. Organic geochemical studies of modern microbial mats from Shark Bay: Part 1: Influence of depth and salinity on lipid biomarkers and their isotopic signatures. Geobiology 12, 469-487.

Pancost, R.D., Bouloubassi, I., Aloisi, G., Sinninghe Damsté, J.S., the Medinaut Shipboard Scientific Party, 2001. Three series of non-isoprenoidal dialkyl glycerol diethers in cold-seep carbonate crusts. Organic Geochemistry 32, 695-707.

Pancost, R.D., Pressley, S., Coleman, J.M., Benning, L.G., Mountain, B.W., 2005. Lipid biomolecules in silica sinters: indicators of microbial biodiversity. Environmental Microbiology 7, 66-77.

Pancost, R.D., Pressley, S., Coleman, J.M., Talbot, H.M., Kelly, S.P., Farrimond, P., Schouten, S., Benning, L., Mountain, B.W., 2006. Composition and implications of diverse lipids in New Zealand geothermal sinters. Geobiology 4, 71-92.

Pancost, R.D., McClymont, E.L., Bingham, E.M., Roberts, Z., Charman, D., Hornibrook, E.R.C., Blundell, A., Chambers, F.M., Lim, K.L.H., Evershed, R.P., 2011. Archaeol as a methanogen biomarker in ombrotrophic bogs. Organic Geochemistry 42, 1279-1287.

Parkhurst, D.L., Appelo, C.A.J., 2013. Description of input and examples for PHREEQC version 3—A computer program for speciation, batch-reaction, one-dimensional transport, and inverse geochemical calculations: U.S.G.S. Techniques and Methods 6, 497pp.

Paulo, C., Dittrich, M., 2013. 2D Raman spectroscopy study of dolomite and cyanobacterial extracellular polymeric substances from Khor Al-Adaid sabkha (Qatar). Journal of Raman Spectroscopy 44, 1563-1569.

Pirretti, M.V., Pagliuca, G., Boni, L., Pistocchi, R., Diamante, M., Gazzotti, T., 1997. Investigation of 4-methyl sterols from cultured dinoflagellate algal strains. Journal of Phycology 33, 61-67.

Proteau, P.J., Gerwick, W.H., Garcia-Pichel, F., Castenholz, R., 1993. The structure of scytonemin, an ultraviolet sunscreen pigment from the sheaths of cyanobacteria. Experientia 49, 825-829.

Rath, J., Mandal, S., Adhikary, S.P., 2012. Salinity induced synthesis of UV-screening compound scytonemin in the cyanobacterium *Lyngbya aestuarii*. Journal of Photochemistry and Photobiology. B. Biology 115, 5-8.

Revsbech, N.P., Jørgensen, B.B., Blackburn, T.H., 1983. Microelectrode studies of the photosynthesis and O_2, H_2S, and pH profiles of a microbial mat. Limnology and Oceanography 28, 1062-1074.

Richlen, M.L., Morton, S.L., Jamali, E.A., Rajan, A., Anderson, D.M., 2009. The catastrophic 2008–2009 red tide in the Arabian Gulf region, with observations on the identification and phylogeny of the fish-killing dinoflagellate *Cochlodinium polykrikoides*. Harmful Algae 9, 163-172.

Robinson, N., Eglinton, G., Brassell, S.C., 1984. Dinoflagellate origin for sedimentary 4α-methylsteroids and 5α(H)-stanols. Nature 308, 439-442.

Rohmer, M., Bouvier-Nave, P., Ourisson, G., 1984. Distribution of hopanoid triterpenes in prokaryotes. Journal of General Microbiology 130, 1137-1150.

Rontani, J.-F., Combe, I., Giral, P.J.-P., 1990. Abiotic degradation of free phytol in the water column: a new pathway for the production of acyclic isoprenoids in the marine environment. Geochimica et CosmochimicaActa 54, 1307-1313.

Rontani, J.-F., Volkman, J.K., 2005. Lipid characterization of coastal hypersaline cyanobacterial mats from the Camargue (France). Organic Geochemistry 36, 251-272.

Roux, J.M., 1996. Production of polysaccharide slime by microbial mats in the hypersaline environment of a Western Australian solar saltfield. International Journal of Salt Lake Research 5, 103-130.

Rowland, S.J., 1990. Production of acyclic isoprenoid hydrocarbons by laboratory maturation of methanogenic bacteria. Organic Geochemistry 15, 9-16.

Schirmer, A., Rude, M.A., Li, X., Popova, E., Del Cardayre, S.B., 2010. Microbial biosynthesis of alkanes. Science 329, 559-562.

Schmidt, T.M., Arieli, B., Cohen, Y., Padan, E., Strohl, W.R., 1987. Sulfur metabolism in *Beggiatoa alba*. Journal of Bacteriology 169, 5466-5742.

Schouten, S., van der Meer, M.T.J., Hopmans, E.C., Rijpstra, W.I.C., Reysenbach, A.-L., Ward, D.M., Sinninghe Damsté, J.S., 2007. Applied and Environmental Microbiology 73, 6181-6191.

Schouten, S., Hopmans, E.C., Sinninghe Damsté, J.S., 2013. The organic geochemistry of glycerol dialkyl glycerol tetraether lipids: a review. Organic Geochemistry 54, 19-61.

Sherf, A.-K., Rullkötter, J., 2009. Biogeochemistry of high salinity microbial mats – Part 1: Lipid composition of microbial mats across intertidal flats of Abu Dhabi, United Arab Emirates. Organic Geochemistry 40, 1018-1028.

Shearman, D.J., Skipwith, P.A., 1965. Organic matter in Recent and ancient limestones and its role in their diagenesis. Nature 208, 1310-1311.

Shinn, E.A., 1972. Worm and algal-built columnar stromatolites in the Persian Gulf. Journal of Sedimentary Petrology 42, 837-840.

Shinn, E.A., 2011. Interplay between Holocene sedimentation and diagenesis, and implications for hydrocarbon exploitation: return to the sabkha of Ras Umm Said, Qatar. In: Kendall, C.G.St.C., Alsharhan, A.S., Jarvis, I. (Eds), Quaternary Carbonate and Evaporite Sedimentary Facies and their Ancient Analogues. IAS Special Publication 43, 133-148.

Sinninghe Damsté, J.S., Baas, M., Geenevasen, J.A.J., Kenig, F., 2005. Structural identification of sedimentary C_{21} and C_{22} highly branched isoprenoid alkanes. Organic Geochemistry 36, 511-517.

Sinninghe Damsté, J.S., Rijpstra, W.I.C., Hopmans, E.C., Weijers, J.W.H., Foesel, B.U., Overmann,

J., Dedysh, S.N., 2011. 13,16-Dimethyl octacosanedioic acid (iso-diabolic acid), a common membrane-spanning lipid of Acidobacteriasubdivisions 1 and 3. Applied and Environmental Microbiology 77, 4147-4154.

Słowakiewicz M., Pancost, R.D., Thomas, L., Tucker, M.E., Ooi, S.M.D., Whitaker, F., 2014. Holocene intertidal microbial mats of Qatar and their implications for petroleum source rock formation in carbonate-siliciclastic-evaporite systems. International Petroleum Technology Conference, 17400.

Stal, L.J., 2012. Ecology of Cyanobacteria II. Springer, The Netherlands, 760 pp.

Strohmenger, C.J., Jameson, J., 2015. Modern coastal systems of Qatar as analogues for arid climate carbonate reservoirs: improving geological and reservoir modelling. First Break 33, 41-50.

Tornabene, T.G., Langworthy, T.A., Holzer, G., Oró, J., 1979. Squalenes, phytanes and other isoprenoids as major neutral lipids of methanogenic and themoacidophilic 'Archaebacteria'. Journal of Molecular Evolution 13, 73-83.

Tucker, M.E. (Ed.) 1988. Techniques in Sedimentology. Blackwell Science, Oxford, 394pp.

Tucker, M.E., Wright, P., 1990. Carbonate sedimentology. Blackwell Science, Oxford, 498pp.

van Dongen, B.E., Roberts, A.P., Schouten, S., Jiang, W.-T., Florindo, F., Pancost, R.D., 2007. Formation of iron sulphide nodules during anaerobic oxidation of methane. Geochimica et Cosmochimica Acta 71, 5155-5167.

Villanueva, L., Navarreta, A., Urmeneta, J., White, D.C., Guerrero, R., 2007. Analysis of diurnal and vertical microbial diversity in a marine cyanobacterial mat. FEMS Microbiology Ecology 74, 59-72.

Vinçon-Laugier, A., Grossi, V., Pacton, M., Escarguel, G., Cravo-Laureau, C., 2016. The alkyl glycerol either lipid composition of heterotrophic sulfate reducing bacteria strongly depends on growth substrate. Organic Geochemistry 98, 141-154.

Volkman, J.K., 1986. Biological marker compounds as indicators of the depositional environments of petroleum source rocks. In: Fleet, A.J., Kelts, K., Talbot, M.R. (Eds), Petroleum Source Rocks. Geological Society London Special Publication 40, 103-122.

Volkman, J.K., Maxwell, J.R., 1986. Acyclic isoprenoids as biological markers. In: Johns, R.B. (Ed.), Biological Markers in the Sedimentary Record. Methods in Geochemistry and Geophysics 24, 1-42.

Volkman, J.K., Rijpstra, W.I.C., de Leeuw, J.W., Mansour, M.P., Jackson, A. E., Blackburn, S.I., 1999. Sterols four dinoflagellates from the genus *Prorocentrum*. Phytochemistry 52, 659–668.

Wakeham, S.G., Ertel, J.R., 1988. Diagenesis of organic matter in suspended particles and sediments in the Cariaco Trench. Organic Geochemistry 13, 815-822

Wakeham, S.G., 1989. Reduction of stenols to stanols in particulate matter at oxic-anoxic boundaries in sea water. Nature 342, 787-790.

Warren, J.K., 2006. Evaporites: Sediments, Resources and Hydrocarbons. Springer, Berlin, 1036 pp.

Weijers, J.W.H., Schouten, S., van der Linden, M., Van Geel, B., Sinninghe Damsté, J.S., 2004. Water table related variations in the abundance of intact archaeal membrane lipids in a Swedish peat bog. FEMS Microbiology Letters 239, 51-56.

Weijers, J.W.H., Panoto, E., van Bleijswijk, J., Schouten, S., Balk, M., Stams, A.J.M., Rijpstra, W.I.C., Sinninghe Damsté, J.S., 2009. Constraints on the biological source(s) of the orphan branched tetraether membrane lipids. Geomicrobiology Journal 26, 402–414.

Weijers, J.W.H., Wiesenberg, G.L.B., Bol, R., Hopmans, E.C., Pancost, R.D., 2010. Carbon isotopic composition of branched tetraether membrane lipids in soils suggest a rapid turnover and a heterotrophic life style of their source organism(s). Biogeosciences 7, 2959–2973.

Whitaker, F., Ooi, S.M.D., Jameson, J., Strohmenger, C.J., 2014. Origins of evaporites in a Holocene mixed clastic and carbonate coastal sabkha: Preliminary hydrological and geochemical data from Mesaieed sabkha, Qatar. International Petroleum Technology Conference, 17567.

Wieland, A., Pape, T., Möbius, J., Klock, J.-H., Michaelis, W., 2008. Carbon pools and isotopic trends in a hypersaline cyanobacterial mat. Geobiology 6, 171-186.

Zeng, Y.B., Ward, D.M., Brassell, S.C., Eglinton, G., 1992. Biogeochemistry of hot spring environments. 2. Lipid compositions of Yellowstone (Wyoming, U.S.A.) cyanobacterial and *Chloroflexus* mats. Chemical Geology 95, 327-345.

Zelles, L., Bai, Q.Y., Rackwitz, R., Chadwick, D., Beese, F., 1995. Determination of phospholipid- and lipopolysaccharide-derived fatty acids as an estimate of microbial biomass and community structures in soils. Biology and Fertility of Soils 19, 115-123.

Zelles, L., 1997. Phospholipid fatty acid profiles in selected members of soil microbial communities. Chemosphere 35, 275-294.

Zeng, Y.B., Ward, D.M., Brassell, S.C., Eglinton, G., 1992. Biogeochemistry of hot spring environments. 2. Lipid compositions of Yellowstone (Wyoming, USA) cyanobacterial and *Chloroflexus* mats. Chemical Geology 95, 327–345.

Zhang, C.L., Pancost, R.D., Qian, Y., Sassen, R., Macko, S.A., 2003. Archaeal lipid biomarkers and isotopic evidence of anaerobic methane oxidation associated with gas hydrates in the Gulf of Mexico. Organic Geochemistry 34, 827–834.

Zhang, C.L., Pearson, A., Li, Y.-L., Mills, G., Wiegel, J., 2006. Thermophilic temperature optimum for crenarchaeol synthesis and its implication for archaeal evolution. Applied and Environmental Microbiology 72, 4419-4422.

Zhang, C.L., Wang, J., Dodsworth, J., Williams, A.J., Zhu, C., Hinrichs, K.-U., Zheng, F., Hedlund, B.P., 2013. In situ production of branched glycerol dialkyl glycerol tetraethers in a great basin hot spring (USA). Frontiers in Microbiology 4, 181.

Zheng, Y., Singarayer, J.S., Cheng, P., Yu, X.F., Valdes, P.J., Pancost, R.D., 2014. Holocene variations in peatland methane cycling associated with the Asian summer monsoon system. Nature Communications 5, 4631.

Zhu, C., Wagner, T., Talbot, H.M., Weijers, J.W.H., Pan, J.-M., Pancost, R.D., 2013. Mechanistic controls on diverse fates of terrestrial organic components in the East China Sea. Geochimica et Cosmochimica Acta 117, 129-143.

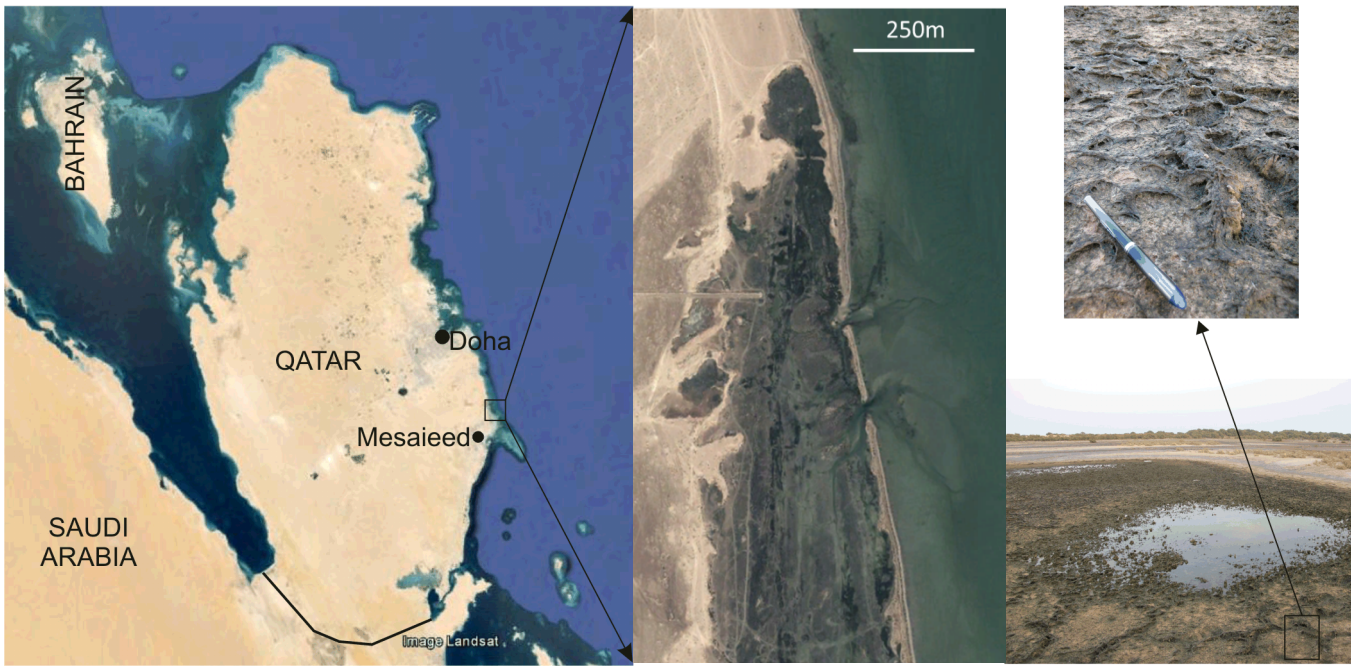

Fig. 1. Google Earth image (2013) of study area (N 25°3'3.29" E 51°36'41.82") and details of lagoon and microbial mat in northern part of Mesaieed.

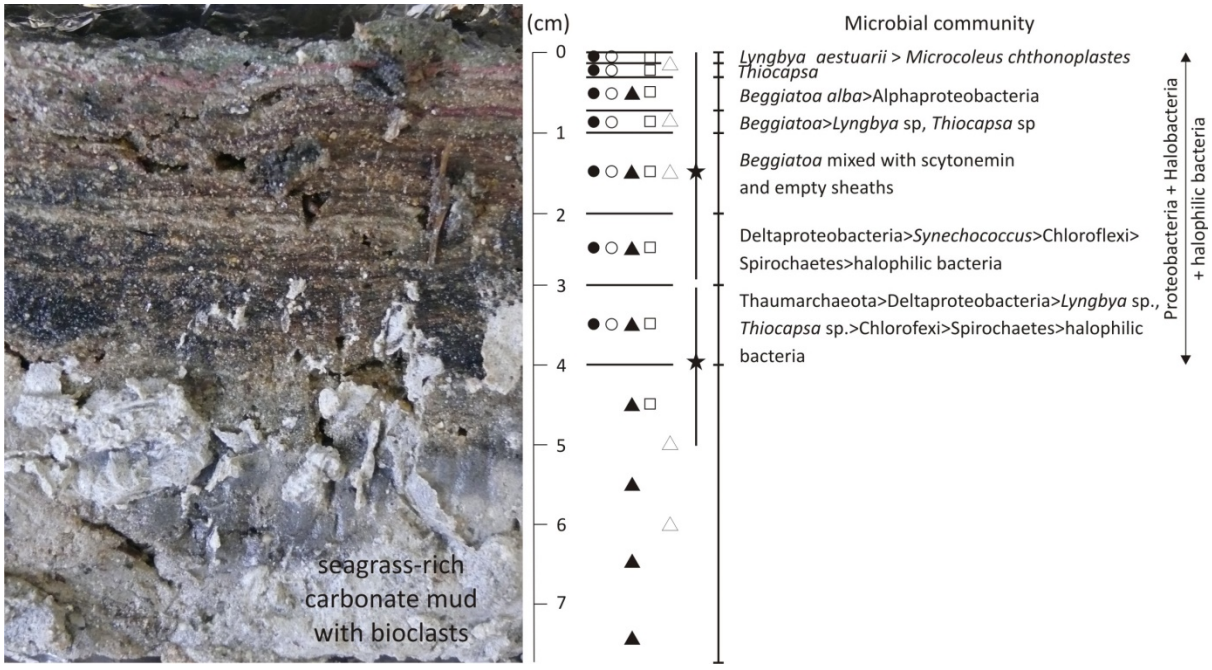

Fig. 2. Sample of a mesohaline microbial mat from Mesaieed, eastern Qatar, showing colour zonation of the layers studied. Sampling intervals for biomarkers (filled circles), microbiology (open circles), pore water chemistry (triangles), palynology (stars), bulk chemistry (squares) and carbon and oxygen isotopes (open triangles) are shown. SRB – sulfate-reducing bacteria.

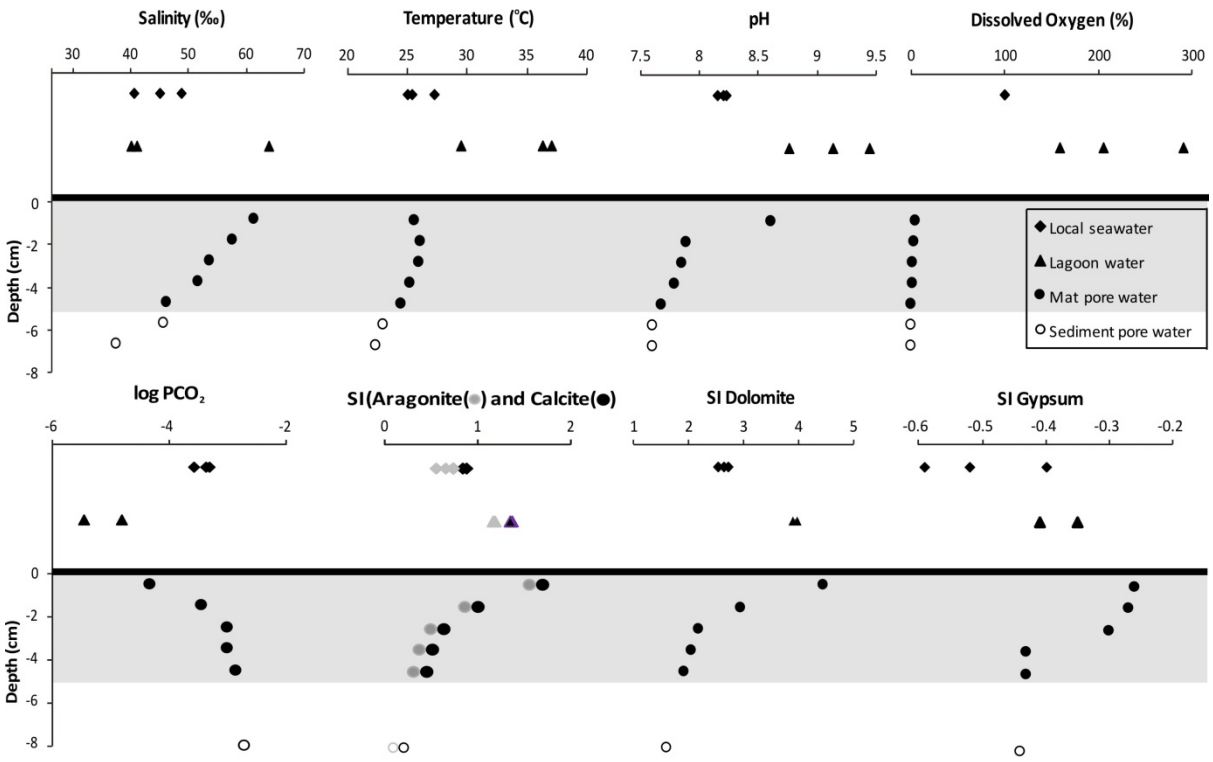

Fig. 3. (a) Salinity, temperature, pH and dissolved O_2 measured in situ. Grey band represents microbial mat; (b) $_PCO_2$ and saturation indices (SI) with respect to aragonite, calcite, dolomite and gypsum.

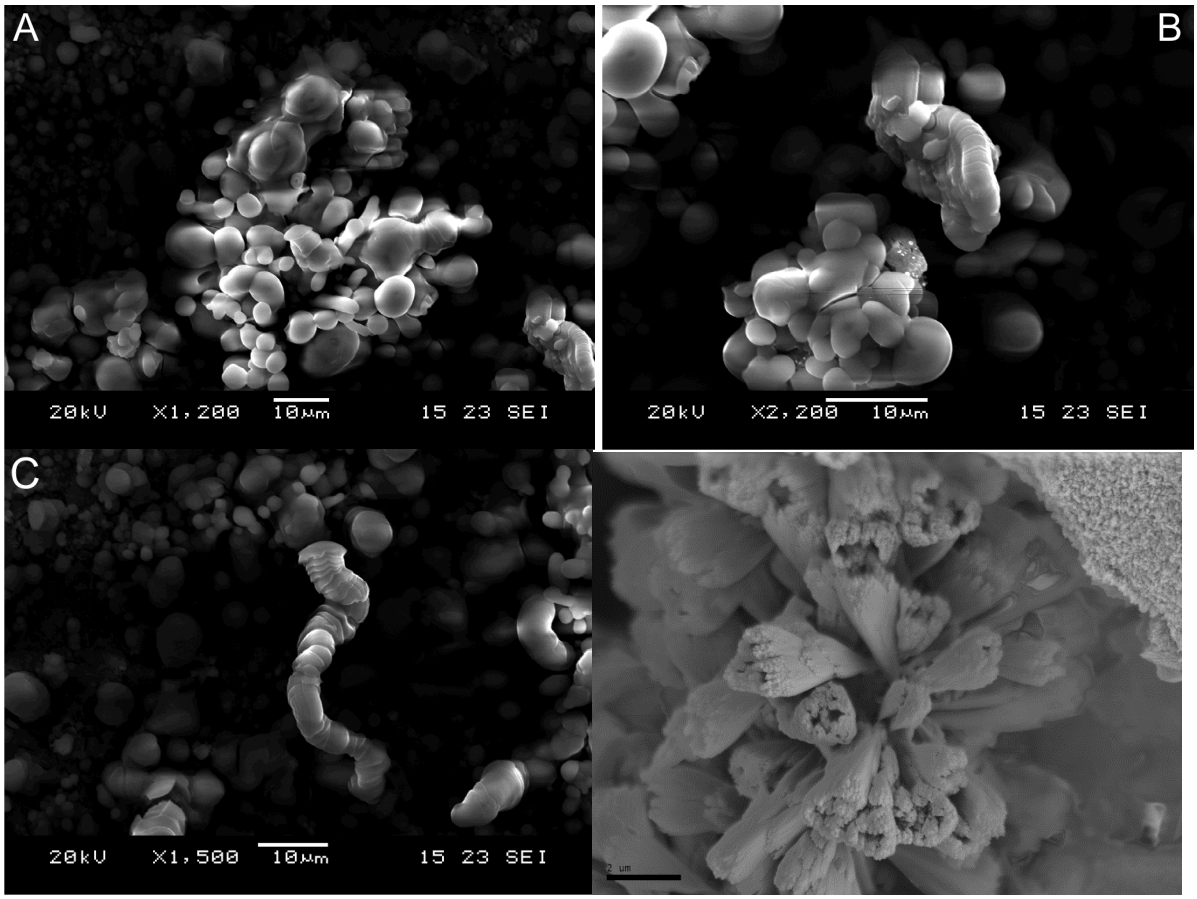

Fig. 4. SEM photographs of material left on glass slide, deposited out of suspension, after OM of mat dissolved in sodium hypochlorite. (a) and (b) – Spheroids of various shapes and sizes, with smooth surface. (c) – Curious elongate assemblage of nested shapes, probably a halophilic bacterium. (d) – dumbbell shaped carbonate particles with a wheat sheaf arrangement of crystallites at the end, scale bar 2 μm.

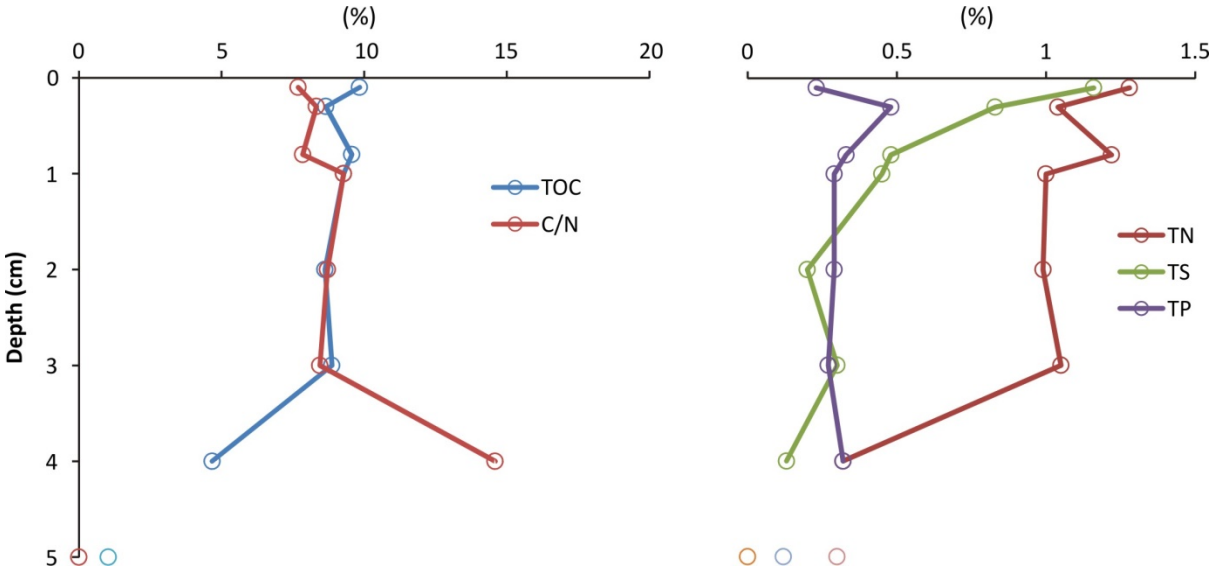

Fig. 5. TOC, C/N, TN, TS and TP distributions in Mesaieed microbial mat and carbonate mud.

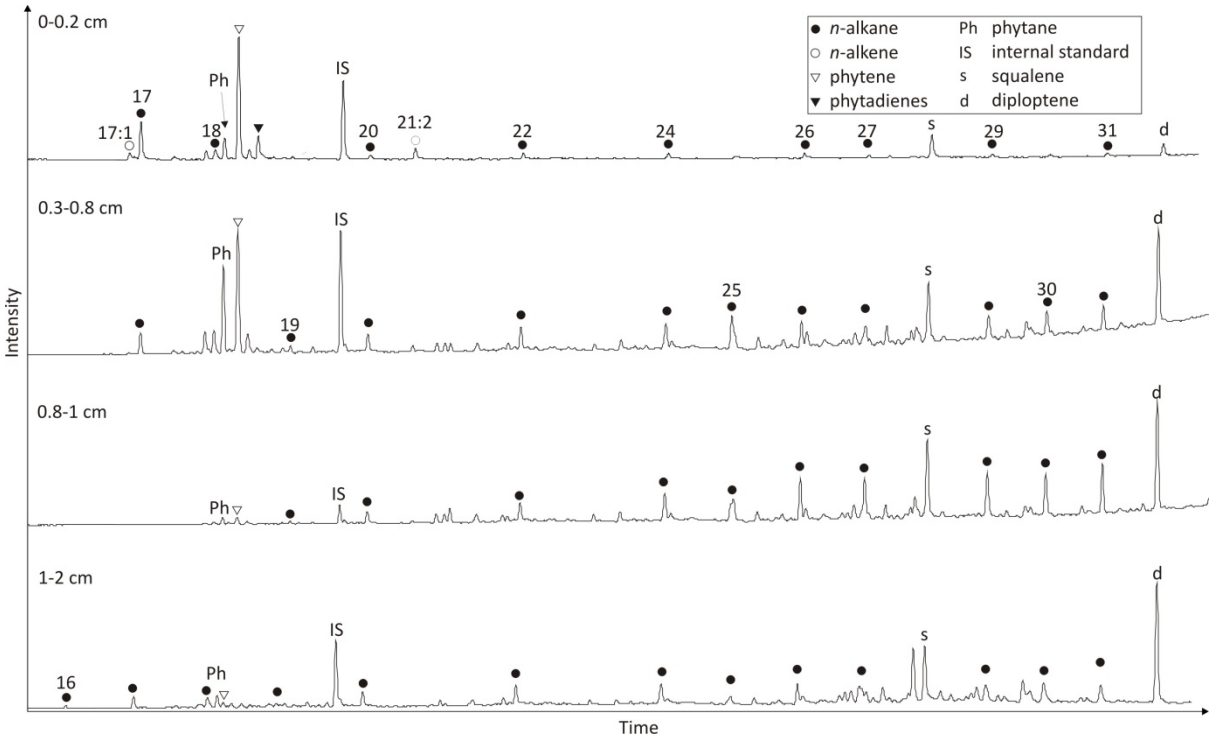

Fig. 6. Partial TIC chromatogram of neutral apolar fractions from layers within the upper 2 cm of the Mesaieed microbial mat, showing *n*-alkanes (solid dots, with numbers denoting carbon chain length) and other major hydrocarbons (IS, internal standard). Several isomers of phytadienes are observed.

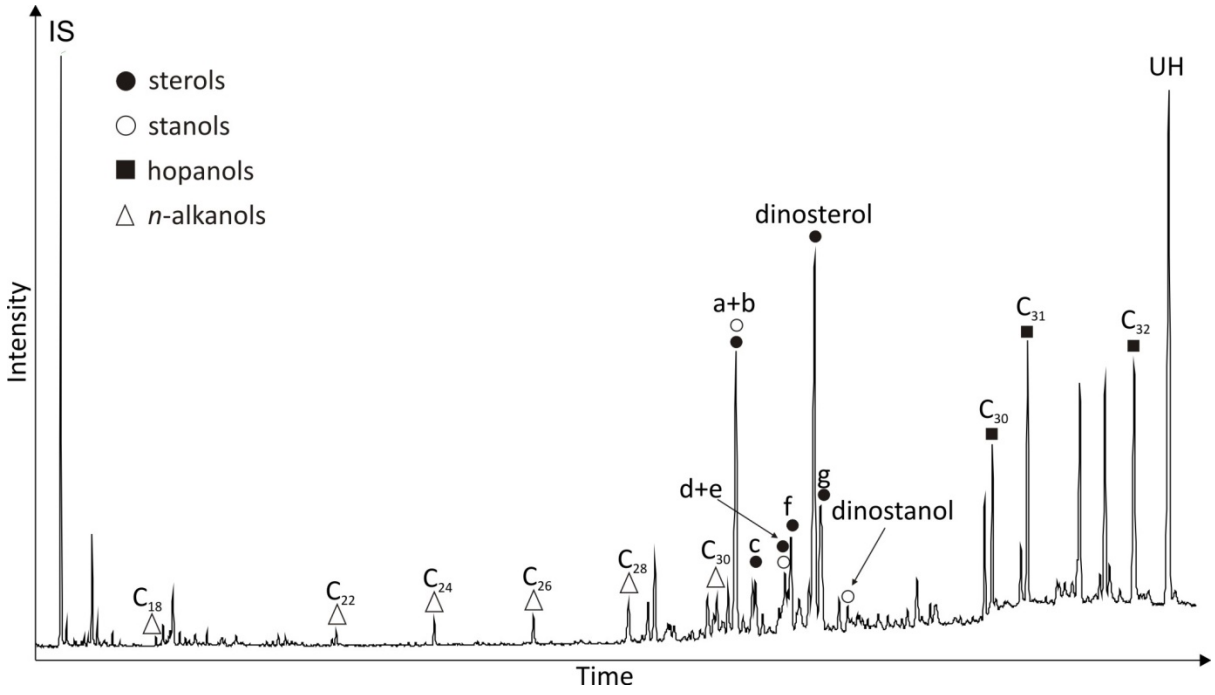

Fig. 7. Partial TIC chromatogram of neutral polar fraction of mat from depth of 0.8 cm, showing sterols (filled circles), stanols (open circles) and hopanoids (filled squares). IS, internal standard; a, cholest-5-en-3β-ol; b, 5α-cholestan-3β-ol; c, 24-methylcholesta-5,22E-dien-3β-ol, d, 24-methylcholest-5-en-3β-ol; e, 24-methyl-5α-cholestan-3β-ol; f, 24-ethylcholesta-5,22E-dien-3β-ol; g, 24-ethylcholest-5-en-3β-ol; UH, unknown hopanoid.

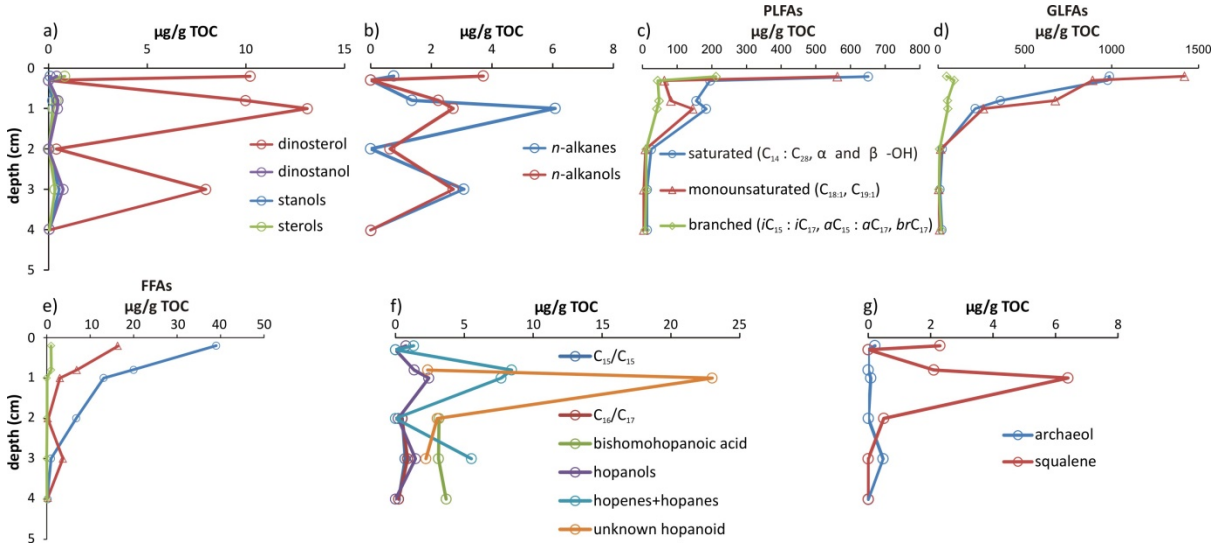

Fig. 8. Distributions of (a) $\Sigma C_{27\text{-}28}$ stanols and dinostanol, $\Sigma C_{27\text{-}29}$ sterols and dinosterol; (b) ΣC_{20}-C_{31} *n*-alkanes and ΣC_{22}-C_{30} *n*-alkanols; saturated, unsaturated and branched PLFAs (c), GLFAs (d) and FFAs (e); (f) DAGEs (C_{15}/C_{16}; C_{16}/C_{17}), $\Sigma(C_{30\text{-}32}$ hopanols), unknown hopanoid, C_{32} bishomohopanoic acid, $\Sigma(C_{27\text{-}31}$ hopanes + $C_{28\text{-}31}$ hopenes + diploptene); and (g) squalene and archaeol within Mesaieed microbial mat.

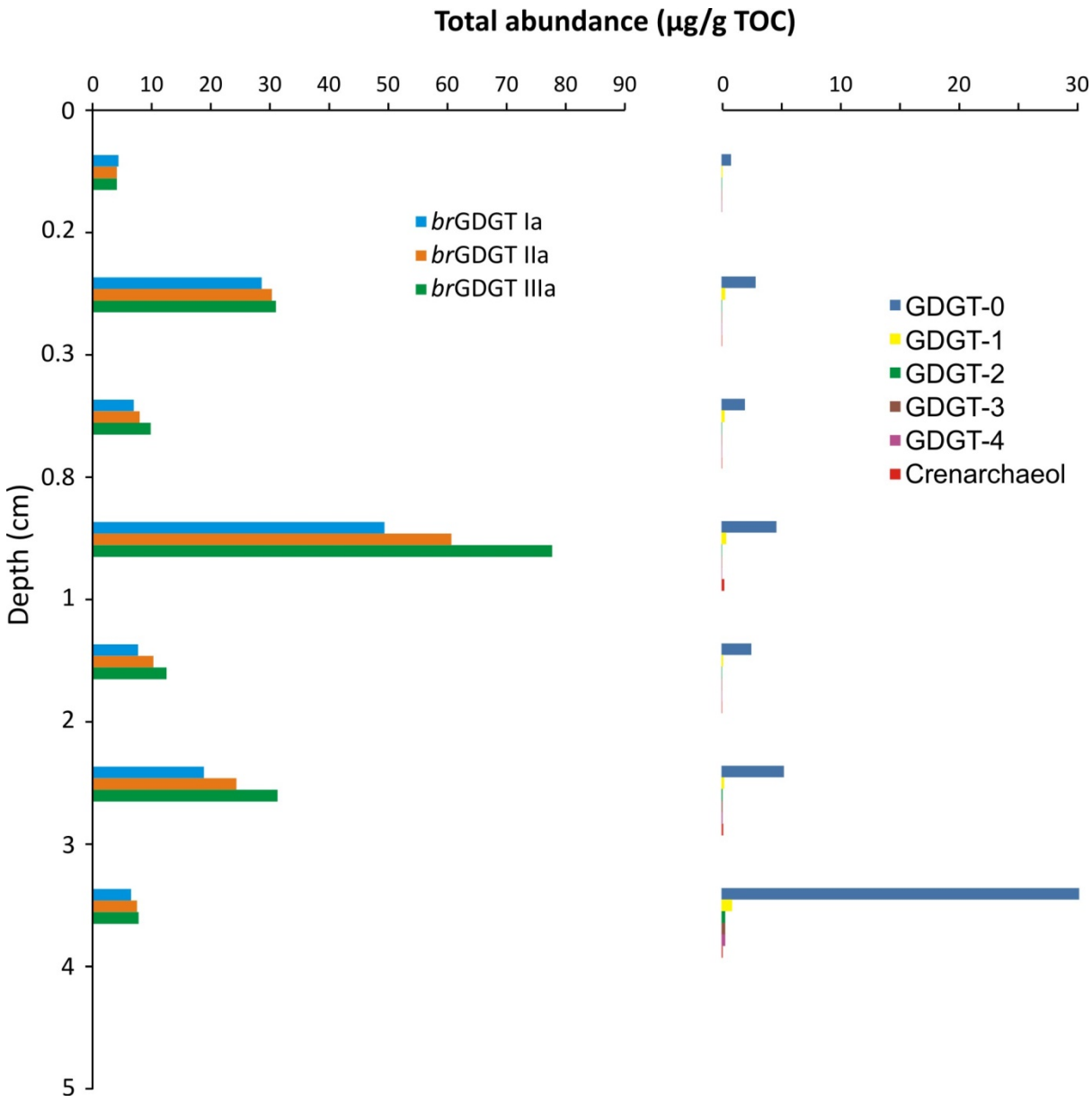

Fig. 9. Summed glycolipidic and phospholipidic isoprenoid (GDGT-0 to GDGT-4 and crenarchaeol) and branched (Ia-IIIa) GDGT distributions with depth from Mesaieed microbial mat.

Table 1

Stable isotope data (‰ PDB) for carbonate from within the microbial mat and from the sediment below.

Depth (cm)	$\delta^{13}C$	$\delta^{18}O$
0-0.2	-2.94	-2.08
0.8-1	-2.04	-1.05
1-2	-1.93	-0.08
5	1.61	1.01
6	1.49	0.54

Table 2

Carbon preference index (CPI) and concentrations (μg/g TOC) of hydrocarbons (hydrocarbons > 3 cm depth were not detected) vs depth (cm). nd – not determined.

Depth	*n*-Alkanes[a]	Phytene	Phytane	Squalene	Sterols[b]	Stanols[c]	Hopanols[d]	Diploptene	UH[e]	CPI
0-0.2	7.5	11.2	2.1	2.3	11.02	0.5	0.76	1.32	nd	0.5
0.3-0.8	6.95	0.5	2.7	2.1	10.37	0.68	1.36	2.71	2.34	1.7
0.8-1	16.73	0.1	0.3	6.4	13.34	0.67	2.42	6.08	23	0.8
1-2	nd	nd	nd	nd	0.43	0.03	0.2	nd	3.03	nd
2-3	4	0.1	0.01	0.5	8.29	1.27	1.45	3.07	2.21	0.9
3-4	nd	nd	nd	nd	nd	nd	nd	nd	nd	nd

[a] $\Sigma C_{16\text{-}31}$; [b]$\Sigma C_{27\text{-}29}$ + dinosterol; [c]$\Sigma C_{27\text{-}29}$ + dinostanol; [d]$\Sigma C_{30\text{-}32}$; [e]unknown hopanoid.

Table S1

TOC and total bulk values for N, S, H and P as well as TOC vs N ratio in Mesaieed microbial mat.

Depth (cm)	TOC (%)	N (%)	S (%)	P (%)	C/N
0-0.1	9.8	1.3	1.2	0.25	7.7
0.2-0.3	8.7	1.0	0.8	0.5	8.3
0.3-0.8	9.8	1.2	0.5	0.3	7.8
0.8-1	9.3	1.0	0.5	0.3	9.3
1-2	8.6	1.0	0.2	0.3	8.7
2-3	8.9	1.1	0.3	0.3	8.4
3-4	4.7	0.3	0.1	0.3	14.6
4-5	1.0	<0.1	0.1	0.3	>10